Eur. Phys. J. C 10, 27–43 (1999)
Digital Object Identifier (DOI) 10.1007/s100529900082

THE EUROPEAN PHYSICAL JOURNAL C

Testing Higgs self-couplings at e^+e^- linear colliders

A. Djouadi[1], W. Kilian[2], M. Mühlleitner[3], P.M. Zerwas[3]

[1] Lab. de Physique Mathématique, Université Montpellier, F-34095 Montpellier Cedex 5, France
[2] Institut für Theoretische Teilchenphysik, Universität Karlsruhe, D-76128 Karlsruhe, Germany
[3] Deutsches Elektronen-Synchrotron DESY, D-22603 Hamburg, Germany

Received: 3 March 1999 / Published online: 15 July 1999

Abstract. To establish the Higgs mechanism *sui generis* experimentally, the self-energy potential of the Higgs field must be reconstructed. This task requires the measurement of the trilinear and quadrilinear self-couplings, as predicted, for instance, in the Standard Model or in supersymmetric theories. The couplings can be probed in multiple Higgs production at high-luminosity e^+e^- linear colliders. Complementing earlier studies to develop a coherent picture of the trilinear couplings, we have analyzed the production of pairs of neutral Higgs bosons in all relevant channels of double Higgs-strahlung, associated multiple Higgs production and WW/ZZ fusion to Higgs pairs.

1 Introduction

1. The Higgs mechanism [1] is a cornerstone in the electroweak sector of the Standard Model (SM) [2]. The electroweak gauge bosons and the fundamental matter particles acquire masses through the interaction with a scalar field. The self-interaction of the scalar field leads to a non-zero field strength $v = (\sqrt{2}G_F)^{-1/2} = 246$ GeV in the ground state, inducing the spontaneous breaking of the electroweak $\mathrm{SU(2)_L \times U(1)_Y}$ symmetry down to the electromagnetic $\mathrm{U(1)_{EM}}$ symmetry.

To establish the Higgs mechanism *sui generis* experimentally, the characteristic self-energy potential of the Standard Model,

$$V = \lambda \left[|\varphi|^2 - \tfrac{1}{2}v^2\right]^2 \tag{1}$$

with a minimum at $\langle\varphi\rangle_0 = v/\sqrt{2}$, must be reconstructed once the Higgs particle will have been discovered. This experimental task requires the measurement of the trilinear and quadrilinear self-couplings of the Higgs boson. The self-couplings are uniquely determined in the Standard Model by the mass of the Higgs boson which is related to the quadrilinear coupling λ by $M_H = \sqrt{2\lambda}v$. Introducing the physical Higgs field H,

$$\varphi = \frac{1}{\sqrt{2}}\begin{bmatrix} 0 \\ v+H \end{bmatrix} \tag{2}$$

the trilinear vertex of the Higgs field H is given by the coefficient

$$\lambda_{HHH} = 3M_H^2/M_Z^2 \tag{3}$$

in units of $\lambda_0 = M_Z^2/v$, while the quadrilinear vertex carries the coefficient

$$\lambda_{HHHH} = 3M_H^2/M_Z^4 \tag{4}$$

in units of λ_0^2; numerically, $\lambda_0 = 33.8$ GeV. For a Higgs mass $M_H = 110$ GeV, the trilinear coupling amounts to $\lambda_{HHH}\lambda_0/M_Z = 1.6$ for a typical energy scale M_Z, whereas the quadrilinear coupling $\lambda_{HHHH}\lambda_0^2 = 0.6$ is suppressed with respect to the trilinear coupling by a factor close to the size of the weak gauge coupling.

The trilinear Higgs self-coupling can be measured directly in pair-production of Higgs particles at hadron and high-energy e^+e^- linear colliders. Several mechanisms that are sensitive to λ_{HHH} can be exploited for this task. Higgs pairs can be produced through double Higgs-strahlung off W or Z bosons [3,4], WW or ZZ fusion [4–8]; moreover through gluon-gluon fusion in pp collisions [9–11] and high-energy $\gamma\gamma$ fusion [4,5,12] at photon colliders. The two main processes at e^+e^-colliders are double Higgs-strahlung and WW fusion:

$$\begin{aligned} &\text{double Higgs-strahlung:} && e^+e^- \xrightarrow[Z]{} ZHH \\ &WW \text{ double-Higgs fusion:} && e^+e^- \xrightarrow[WW]{} \bar{\nu}_e\nu_e HH \end{aligned} \tag{5}$$

The ZZ fusion process of Higgs pairs is suppressed by an order of magnitude since the electron-Z couplings are small. Generic diagrams for the above two processes are depicted in Fig. 1.

With values typically of the order of a few fb and below, the cross sections are small at e^+e^- linear colliders for masses of the Higgs boson in the intermediate mass range. High luminosities are therefore needed to produce a sufficiently large sample of Higgs-pair events and to isolate the signal from the background.

2. If light Higgs bosons with masses below about 130 GeV will be found, the Standard Model is likely embedded in a supersymmetric theory. The minimal supersymmetric

double Higgs-strahlung: $e^+e^- \to ZHH$

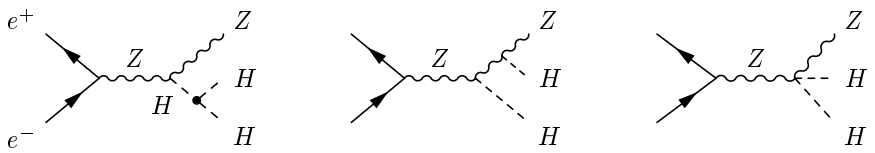

WW double-Higgs fusion: $e^+e^- \to \bar{\nu}_e \nu_e HH$

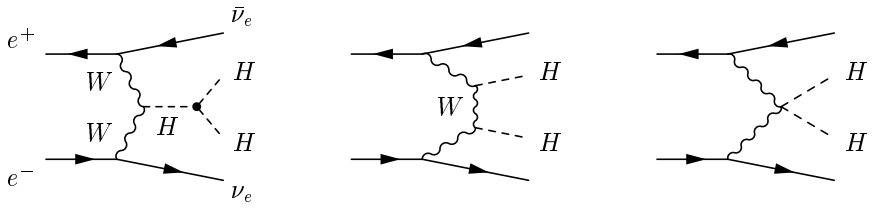

Fig. 1. Processes contributing to Higgs-pair production in the Standard Model at e^+e^- linear colliders: double Higgs-strahlung and WW fusion (generic diagrams)

extension of the Standard Model (MSSM) includes two iso-doublets of Higgs fields φ_1, φ_2 which, after three components are absorbed to provide masses to the electroweak gauge bosons, gives rise to a quintet of physical Higgs boson states: h, H, A, $H^\pm$ [13]. While a strong upper bound of about 130 GeV can be derived on the mass of the light CP-even neutral Higgs boson h [14,15], the heavy CP-even and CP-odd neutral Higgs bosons H, A, and the charged Higgs bosons $H^\pm$ may have masses of the order of the electroweak symmetry scale v up to about 1 TeV. This extended Higgs system can be described by two parameters at the tree level: one mass parameter which is generally identified with the pseudoscalar A mass M_A, and $\tan\beta$, the ratio of the vacuum expectation values of the two neutral fields in the two iso-doublets.

The general self-interaction potential of two Higgs doublets φ_i in a CP-conserving theory can be expressed by seven real couplings λ_k and three real mass parameters m_{11}^2, m_{22}^2 and m_{12}^2:

$$\begin{aligned} V[\varphi_1,\varphi_2] &= m_{11}^2\varphi_1^\dagger\varphi_1 + m_{22}^2\varphi_2^\dagger\varphi_2 - [m_{12}^2\varphi_1^\dagger\varphi_2 + \text{h.c.}] \\ &+ \tfrac{1}{2}\lambda_1(\varphi_1^\dagger\varphi_1)^2 + \tfrac{1}{2}\lambda_2(\varphi_2^\dagger\varphi_2)^2 + \lambda_3(\varphi_1^\dagger\varphi_1)(\varphi_2^\dagger\varphi_2) \\ &+ \lambda_4(\varphi_1^\dagger\varphi_2)(\varphi_2^\dagger\varphi_1) + \Big\{\tfrac{1}{2}\lambda_5(\varphi_1^\dagger\varphi_2)^2 + [\lambda_6(\varphi_1^\dagger\varphi_1) \\ &+ \lambda_7(\varphi_2^\dagger\varphi_2)]\varphi_1^\dagger\varphi_2 + \text{h.c.}\Big\} \end{aligned} \tag{6}$$

In the MSSM, the λ parameters are given at tree level by

$$\begin{aligned} \lambda_1 = \lambda_2 &= \tfrac{1}{4}(g^2+g'^2) \\ \lambda_3 &= \tfrac{1}{4}(g^2-g'^2) \\ \lambda_4 &= -\tfrac{1}{2}g^2 \\ \lambda_5 = \lambda_6 &= \lambda_7 = 0 \end{aligned} \tag{7}$$

and the mass parameters by

$$\begin{aligned} m_{12}^2 &= \tfrac{1}{2}M_A^2 \sin 2\beta \\ m_{11}^2 &= (M_A^2 + M_Z^2)\sin^2\beta - \tfrac{1}{2}M_Z^2 \\ m_{22}^2 &= (M_A^2 + M_Z^2)\cos^2\beta - \tfrac{1}{2}M_Z^2 \end{aligned} \tag{8}$$

The mass M_A and $\tan\beta$ determine the strength of the trilinear couplings of the physical Higgs bosons, together with the electroweak gauge couplings.

The mass parameters m_{ij}^2 and the couplings λ_i in the potential are affected by top and stop-loop radiative corrections. Radiative corrections in the one-loop leading m_t^4 approximation are parameterized by

$$\epsilon \approx \frac{3G_F m_t^4}{\sqrt{2}\pi^2 \sin^2\beta} \log\frac{M_S^2}{M_t^2} \tag{9}$$

where the scale of supersymmetry breaking is characterized by a common squark-mass value M_S, set 1 TeV in the numerical analyses; if stop mixing effects are modest on the SUSY scale, they can be accounted for by shifting M_S^2 in ϵ by the amount $\Delta M_S^2 = \hat{A}^2[1 - \hat{A}^2/(12M_S^2)]$ where $\hat{A} = -\mu\cot\beta$ denotes the modified trilinear $\tilde{t}$ coupling in the superpotential. The charged and neutral CP-even Higgs boson masses, and the mixing angle α are given in this approximation by

$$\begin{aligned} M_{H^\pm}^2 &= M_A^2 + M_Z^2\cos^2\theta_W \\ M_{h,H}^2 &= \tfrac{1}{2}\Big[M_A^2 + M_Z^2 + \epsilon \\ &\mp \sqrt{(M_A^2+M_Z^2+\epsilon)^2 - 4M_A^2M_Z^2\cos^2 2\beta - 4\epsilon(M_A^2\sin^2\beta + M_Z^2\cos^2\beta)}\Big] \\ \tan 2\alpha &= \tan 2\beta \frac{M_A^2+M_Z^2}{M_A^2 - M_Z^2 + \epsilon/\cos 2\beta} \qquad \text{with} \qquad -\tfrac{\pi}{2} \le \alpha \le 0 \end{aligned} \tag{10}$$

when expressed in terms of the mass M_A and $\tan\beta$.

The set of trilinear couplings between the neutral physical Higgs bosons can be written [14,17] in units of λ_0 as

$$\begin{aligned} \lambda_{hhh} &= 3\cos 2\alpha \sin(\beta+\alpha) + 3\frac{\epsilon}{M_Z^2}\frac{\cos\alpha}{\sin\beta}\cos^2\alpha \\ \lambda_{Hhh} &= 2\sin 2\alpha\sin(\beta+\alpha) - \cos 2\alpha\cos(\beta+\alpha) \\ &\quad + 3\frac{\epsilon}{M_Z^2}\frac{\sin\alpha}{\sin\beta}\cos^2\alpha \\ \lambda_{HHh} &= -2\sin 2\alpha\cos(\beta+\alpha) - \cos 2\alpha\sin(\beta+\alpha) \end{aligned}$$

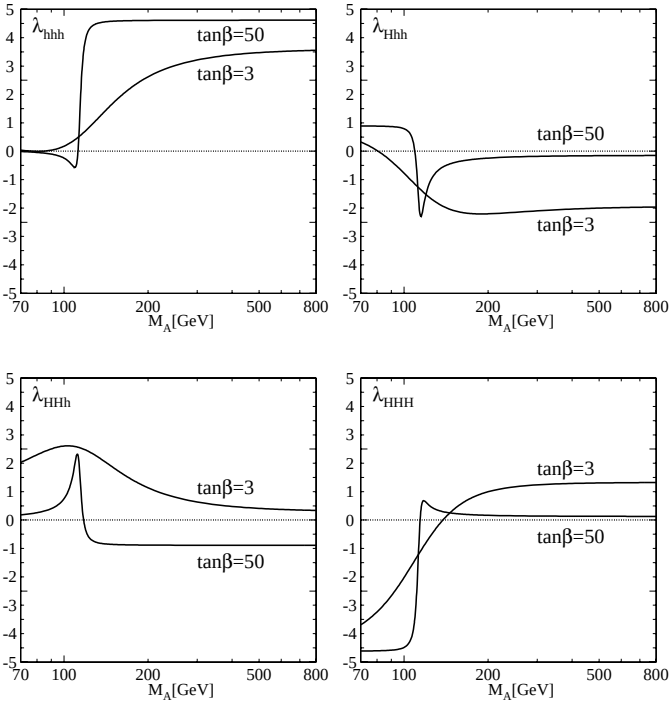

Fig. 2. Variation of the trilinear couplings between CP-even Higgs bosons with M_A for $\tan\beta = 3$ and 50 in the MSSM; the region of rapid variations corresponds to the h/H cross-over region in the neutral CP-even sector

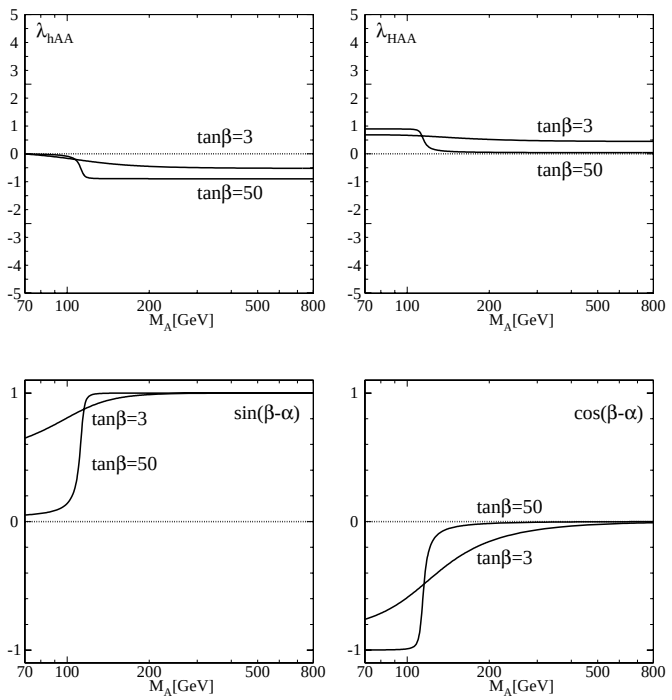

Fig. 3. Upper set: Variation of the trilinear scalar couplings between CP-even and CP-odd Higgs bosons with M_A for $\tan\beta = 3$ and 50 in the MSSM. Lower set: ZZh and ZZH gauge couplings in units of the SM coupling

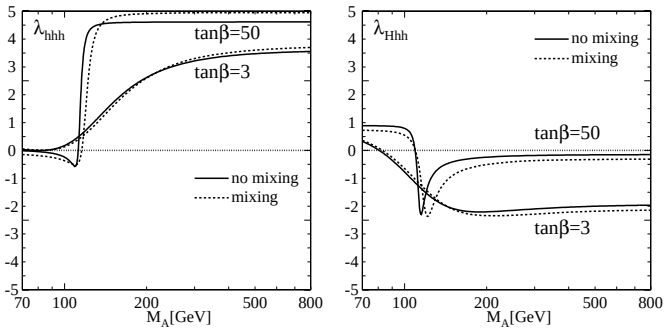

Fig. 4. Modification of the trilinear couplings λ_{hhh} and λ_{Hhh} due to mixing effects for $A = \mu = 1$ TeV

$$
\begin{aligned}
&+3\frac{\epsilon}{M_Z^2}\frac{\cos\alpha}{\sin\beta}\sin^2\alpha \\
\lambda_{HHH} &= 3\cos 2\alpha\cos(\beta+\alpha) + 3\frac{\epsilon}{M_Z^2}\frac{\sin\alpha}{\sin\beta}\sin^2\alpha \\
\lambda_{hAA} &= \cos 2\beta\sin(\beta+\alpha) + \frac{\epsilon}{M_Z^2}\frac{\cos\alpha}{\sin\beta}\cos^2\beta \\
\lambda_{HAA} &= -\cos 2\beta\cos(\beta+\alpha) + \frac{\epsilon}{M_Z^2}\frac{\sin\alpha}{\sin\beta}\cos^2\beta \quad (11)
\end{aligned}
$$

In the decoupling limit $M_A^2 \sim M_H^2 \sim M_{H^\pm}^2 \gg v^2/2$, the trilinear Higgs couplings reduce to

$$
\begin{aligned}
\lambda_{hhh} &\to \frac{3M_h^2}{M_Z^2} \\
\lambda_{Hhh} &\to -\frac{3}{2}|\sin 4\beta| - \frac{3\epsilon}{M_Z^2}\sin\beta\cos\beta \\
\lambda_{HHh} &\to 2 - \frac{3M_h^2}{M_Z^2} + \frac{3\epsilon}{M_Z^2} \\
\lambda_{HHH} &\to \frac{3}{2}|\sin 4\beta| - \frac{3\epsilon}{M_Z^2}\frac{\cos^3\beta}{\sin\beta} \\
\lambda_{hAA} &\to -\frac{M_h^2}{M_Z^2} + \frac{\epsilon}{M_Z^2} \\
\lambda_{HAA} &\to \frac{1}{2}|\sin 4\beta| - \frac{\epsilon}{M_Z^2}\frac{\cos^3\beta}{\sin\beta} \quad (12)
\end{aligned}
$$

with $M_h^2 = M_Z^2\cos^2 2\beta + \epsilon\sin^2\beta$. As expected, the self-coupling of the light CP-even neutral Higgs boson h approaches the SM value in the decoupling limit.

In the subsequent numerical analysis the complete one-loop and the leading two-loop corrections to the MSSM Higgs masses and to the trilinear couplings are included, as presented in [15,16]. Mixing effects due to non-vanishing A, μ parameters primarily affect the light Higgs mass; the upper limit on M_h depends strongly on the size of the mixing parameters, raising this value for $\tan\beta \gtrsim 2.5$ beyond the reach of LEP2, cf. [18]. The couplings however are affected less when evaluated for the physical Higgs masses. The variation of the trilinear couplings with M_A is shown for two values $\tan\beta = 3$ and 50 in Figs. 2 and 3. The region in which the couplings vary rapidly, corresponds to the h/H cross-over region of the two mass branches

in the neutral CP-even sector, cf. (10). The trilinear couplings between h, H and the pseudoscalar pair AA are in general significantly smaller than the trilinear couplings among the CP-even Higgs bosons. Small modifications of the couplings due to mixing effects are illustrated in Fig. 4 (for a detailed discussion of mixing effects see [19]).

In contrast to the Standard Model, resonance production of the heavy neutral Higgs boson H followed by subsequent decays $H \to hh$, plays a dominant role in part of the parameter space for moderate values of $\tan\beta$ and H masses between 200 and 350 GeV, [20]. In this range, the branching ratio, derived from the partial width

$$\Gamma(H \to hh) = \frac{\sqrt{2} G_F M_Z^4 \beta_h}{32\pi M_H} \lambda^2_{Hhh} \qquad (13)$$

is neither too small nor too close to unity to be measured directly. [The decay of either h or H into a pair of pseudoscalar states, $h/H \to AA$, is kinematically not possible in the parameter range which the present analysis is based upon.] If double Higgs production is mediated by the resonant production of H, the total production cross section of light Higgs pairs increases by about an order of magnitude [17].

The trilinear Higgs-boson couplings are involved in a large number of processes at e^+e^- linear colliders [17]:

$$\begin{array}{ll} \text{double Higgs-strahlung:} & e^+e^- \to ZH_iH_j \\ & \text{and } ZAA[H_{i,j} = h, H] \\ \text{triple Higgs production:} & e^+e^- \to AH_iH_j \\ & \text{and } AAA \\ WW \text{ double-Higgs fusion:} & e^+e^- \to \bar{\nu}_e\nu_e H_iH_j \\ & \text{and } \bar{\nu}_e\nu_e AA \end{array} \qquad (14)$$

The trilinear couplings which enter for various final states, cf. Fig. 5, are marked by a cross in the matrix Table 1. While the combination of couplings in Higgs-strahlung is isomorphic to WW fusion, it is different for associated triple Higgs production. If all the cross sections were large enough, the system could be solved for all λ's, up to discrete ambiguities, based on double Higgs-strahlung, Ahh and triple A production ["bottom-up approach"]. This can easily be inferred from the correlation matrix Table 1. From $\sigma(ZAA)$ and $\sigma(AAA)$ the couplings $\lambda(hAA)$ and $\lambda(HAA)$ can be extracted. In a second step, $\sigma(Zhh)$ and $\sigma(Ahh)$ can be used to solve for $\lambda(hhh)$ and $\lambda(Hhh)$; subsequently, $\sigma(ZHh)$ for $\lambda(HHh)$; and, finally, $\sigma(ZHH)$ for $\lambda(HHH)$. The remaining triple Higgs cross sections $\sigma(AHh)$ and $\sigma(AHH)$ provide additional information on the trilinear couplings.

In practice, not all the cross sections will be large enough to be accessible experimentally, preventing the straightforward solution for the complete set of couplings. In this situation however the reverse direction can be followed ["top-down approach"]. The trilinear Higgs couplings can stringently be tested by comparing the theoretical predictions of the cross sections with the experimental results for the accessible channels of double and triple Higgs production.

Table 1. The trilinear couplings between neutral CP-even and CP-odd MSSM Higgs bosons which can generically be probed in double Higgs-strahlung and associated triple Higgs-production, are marked by a cross. The matrix for WW fusion is isomorphic to the matrix for Higgs-strahlung

	double Higgs−strahlung				triple Higgs−production			
λ	Zhh	ZHh	ZHH	ZAA	Ahh	AHh	AHH	AAA
hhh	×				×			
Hhh	×	×			×	×		
HHh		×	×			×	×	
HHH			×				×	
hAA				×	×	×		×
HAA				×		×	×	×

The processes $e^+e^- \to ZH_iA$ and $e^+e^- \to \bar{\nu}_e\nu_e H_iA$ [$H_i = h, H$] of mixed CP-even/CP-odd Higgs final states are generated through gauge interactions alone, mediated by virtual Z bosons decaying to the CP even–odd Higgs pair, $Z^* \to H_iA$. These parity-mixed processes do not involve trilinear Higgs-boson couplings.

3. In this paper we compare different mechanisms for the production of Higgs boson pairs in the Standard Model and in the minimal supersymmetric extension. An excerpt of the results, including comparisons with LHC channels, has been published in [21]. The relation to general 2-Higgs doublet models has recently been discussed in [22]. The analyses have been carried out for e^+e^- linear colliders [23], which are currently designed [24] for a low-energy phase in the range $\sqrt{s} = 500$ GeV to 1 TeV, and a high-energy phase above 1 TeV, potentially extending up to 5 TeV. The small cross sections require high luminosities as foreseen in the TESLA design with targets of $\int \mathcal{L} = 300$ and 500 fb^{-1} *per annum* for $\sqrt{s} = 500$ and 800 GeV, respectively [25]. By analyzing the entire ensemble of multi-Higgs final states as defined in [17], a theoretically coherent picture has been developed for testing the trilinear self-couplings at high-energy colliders. Moreover, the fusion processes are calculated exactly without reference to the equivalent-particle approximation. Experimental simulations of signal and background processes depend strongly on detector properties; they are beyond the scope of the present study which describes the first modest theoretical steps into this area. Crude estimates for final states $e^+e^- \to Z(b\bar{b})(b\bar{b})$ [26] and $e^+e^- \to Z(WW)(WW)$ [27] can however be derived from the existing literature; dedicated analyses of the reducible $Z(b\bar{b})(b\bar{b})$ background channel will be available in the near future [28].

The paper is divided into two parts. In Sect. 2 we discuss the measurement of the trilinear Higgs coupling in the Standard Model for double Higgs-strahlung and WW fusion at e^+e^- linear colliders. In Sect. 3 this program,

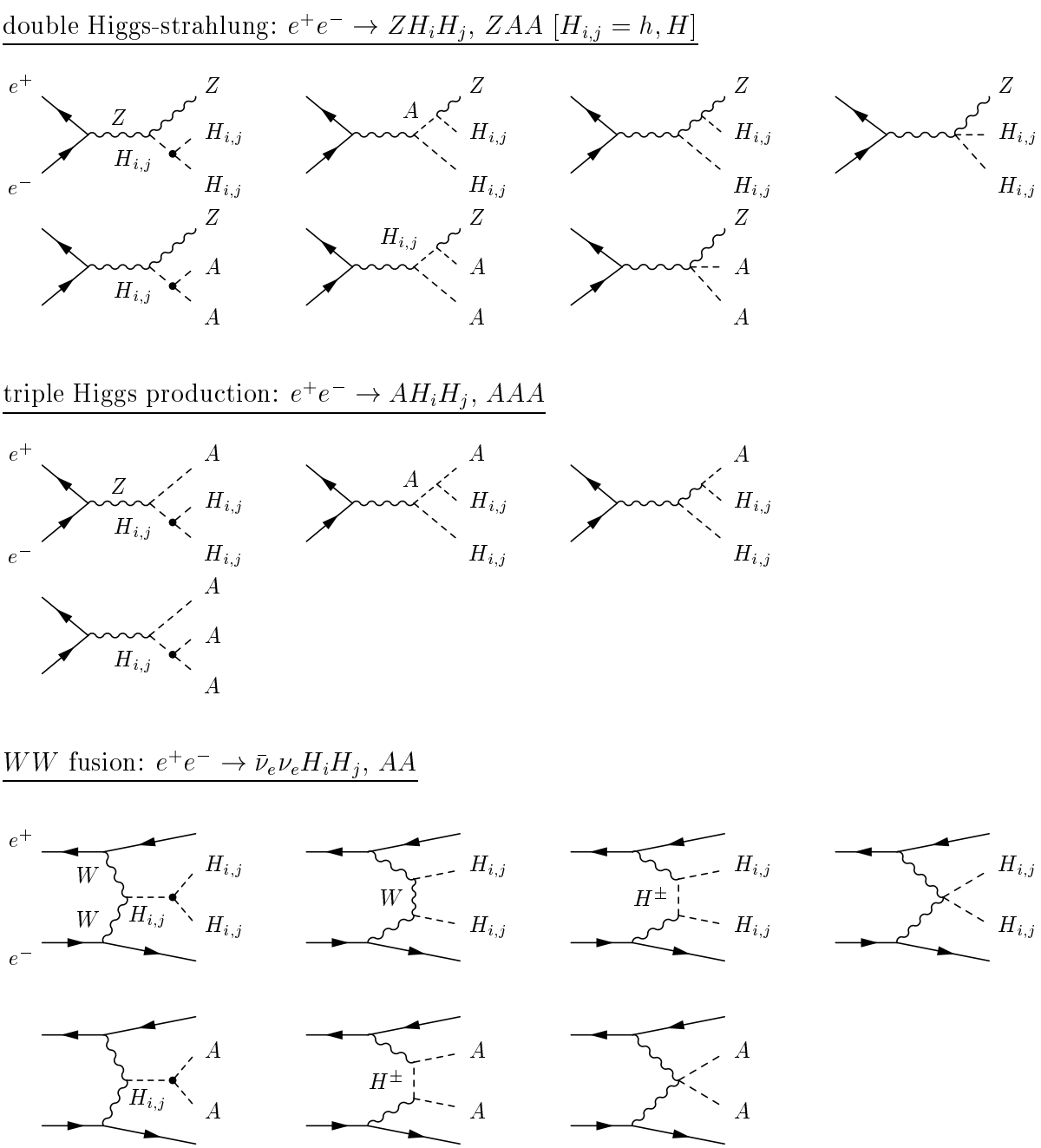

Fig. 5. Processes contributing to double and triple Higgs production involving trilinear couplings in the MSSM

including the triple Higgs production, is extended to the Minimal Supersymmetric Standard Model (MSSM).

2 Higgs pair–production in the standard model

2.1 Double Higgs-strahlung

The (unpolarized) differential cross section for the process of double Higgs-strahlung $e^+e^- \to ZHH$, cf. Fig. 1, can be cast into the form [17]

$$\frac{d\sigma(e^+e^- \to ZHH)}{dx_1 dx_2} = \frac{\sqrt{2}G_F^3 M_Z^6}{384\pi^3 s} \frac{v_e^2 + a_e^2}{(1-\mu_Z)^2}\, \mathcal{Z} \quad (15)$$

after the angular dependence is integrated out. The vector and axial-vector Z charges of the electron are defined as usual, by $v_e = -1 + 4\sin^2\theta_W$ and $a_e = -1$. $x_{1,2} = 2E_{1,2}/\sqrt{s}$ are the scaled energies of the two Higgs particles, $x_3 = 2 - x_1 - x_2$ is the scaled energy of the Z boson, and $y_i = 1 - x_i$; the square of the reduced masses is denoted by $\mu_i = M_i^2/s$, and $\mu_{ij} = \mu_i - \mu_j$. In terms of

these variables, the coefficient $\mathcal{Z}$ may be written as:

$$\mathcal{Z} = \mathfrak{z}^2 f_0 + \frac{1}{4\mu_Z(y_1+\mu_{HZ})}\left[\frac{f_1}{y_1+\mu_{HZ}} + \frac{f_2}{y_2+\mu_{HZ}} + 2\mu_Z \mathfrak{z} f_3\right] + \{y_1 \leftrightarrow y_2\} \quad (16)$$

with

$$\mathfrak{z} = \frac{\lambda_{HHH}}{y_3-\mu_{HZ}} + \frac{2}{y_1+\mu_{HZ}} + \frac{2}{y_2+\mu_{HZ}} + \frac{1}{\mu_Z} \quad (17)$$

The coefficients f_i are given by the following expressions,

$$\begin{aligned}
f_0 &= \mu_Z[(y_1+y_2)^2 + 8\mu_Z]/8 \\
f_1 &= (y_1-1)^2(\mu_Z-y_1)^2 - 4\mu_H y_1(y_1+y_1\mu_Z-4\mu_Z) \\
&\quad + \mu_Z(\mu_Z-4\mu_H)(1-4\mu_H) - \mu_Z^2 \\
f_2 &= [\mu_Z(y_3+\mu_Z-8\mu_H) - (1+\mu_Z)y_1y_2](1+y_3+2\mu_Z) \\
&\quad + y_1y_2[y_1y_2 + 1 + \mu_Z^2 + 4\mu_H(1+\mu_Z)] \\
&\quad + 4\mu_H\mu_Z(1+\mu_Z+4\mu_H) + \mu_Z^2 \\
f_3 &= y_1(y_1-1)(\mu_Z-y_1) - y_2(y_1+1)(y_1+\mu_Z) \\
&\quad + 2\mu_Z(1+\mu_Z-4\mu_H)
\end{aligned} \quad (18)$$

The first term in the coefficient $\mathfrak{z}$ includes the trilinear coupling λ_{HHH}. The other terms are related to sequential Higgs-strahlung amplitudes and the 4-gauge-Higgs boson coupling; the individual terms can easily be identified by examining the characteristic propagators.

Since double Higgs-strahlung is mediated by s-channel Z-boson exchange, the cross section doubles if oppositely polarized electron and positron beams are used.

The cross sections for double Higgs-strahlung in the intermediate mass range are presented in Fig. 6a for total e^+e^- energies of $\sqrt{s} = 500$ GeV, 1 TeV and 1.6 TeV. The cross sections are shown for polarized electrons and positrons $[\lambda_{e^-}\lambda_{e^+} = -1]$; they reduce by a factor of 2 for unpolarized beams. As a result of the scaling behavior, the cross section for double Higgs-strahlung decreases with rising energy beyond the threshold region. The cross section increases with rising trilinear self-coupling in the vicinity of the SM value. The sensitivity to the HHH self-coupling is demonstrated in Fig. 6b for $\sqrt{s} = 500$ GeV and $M_H = 110$ GeV by varying the trilinear coupling $\kappa\lambda_{HHH}$ within the range $\kappa = -1$ and $+2$; the sensitivity is also illustrated by the vertical arrows in Fig. 6a for a variation κ between 1/2 and 3/2. Evidently the cross section $\sigma(e^+e^- \to ZHH)$ is sensitive to the value of the trilinear coupling, which is not swamped by the irreducible background diagrams involving only the Higgs-gauge couplings. While the irreducible background diagrams become more important for rising energies, the sensitivity to the trilinear Higgs coupling is very large just above the kinematical threshold for the ZHH final state as demonstrated in Fig. 6c. Near the threshold the propagator of the intermediate virtual Higgs boson connecting to the two real Higgs bosons through λ_{HHH} in the final state is maximal. The maximum cross section for double Higgs-strahlung is reached at energies $\sqrt{s} \sim 2M_H + M_Z + 200$ GeV, i.e. for Higgs masses in the lower part of the intermediate range at $\sqrt{s} \sim 500$ GeV.

2.2 WW double-Higgs fusion

The WW fusion mechanism in $e^+e^- \to \bar{\nu}_e\nu_e HH$, cf. Fig. 1, provides the largest cross section for Higgs bosons pairs in the intermediate mass range at high e^+e^- collider energies, in particular for polarized beams.

The fusion cross section can roughly be estimated in the equivalent W-boson approximation. The production amplitude for the dominant longitudinal degrees of freedom is given [29] by

$$\begin{aligned}
\mathcal{M}_{LL} = \frac{G_F\hat{s}}{\sqrt{2}}\Bigg\{ & (1+\beta_W^2)\left[1 + \frac{\lambda_{HHH}}{(\hat{s}-M_H^2)/M_Z^2}\right] \\
& + \frac{1}{\beta_W\beta_H}\left[\frac{(1-\beta_W^4) + (\beta_W - \beta_H\cos\theta)^2}{\cos\theta - x_W}\right. \\
& \left. - \frac{(1-\beta_W^4) + (\beta_W + \beta_H\cos\theta)^2}{\cos\theta + x_W}\right]\Bigg\}
\end{aligned} \quad (19)$$

with $\beta_{W,H}$ denoting the W, H velocities in the c.m. frame, and $x_W = (1 - 2M_H^2/\hat{s})/(\beta_W\beta_H)$. $\hat{s}^{1/2}$ is the invariant energy of the WW pair; θ is the Higgs production angle in the c.m. frame of WW. Integrating out the angular dependence, the corresponding total cross section can be derived [17] as

$$\begin{aligned}
\hat{\sigma}_{LL} = & \frac{G_F^2 M_W^4}{4\pi\hat{s}} \frac{\beta_H}{\beta_W(1-\beta_W^2)^2} \\
& \times\Bigg\{(1+\beta_W^2)^2\left[1 + \frac{\lambda_{HHH}}{(\hat{s}-M_H^2)/M_Z^2}\right]^2 \\
& + \frac{16}{(1+\beta_H^2)^2 - 4\beta_H^2\beta_W^2}\left[\beta_H^2(-\beta_H^2 x_W^2 + 4\beta_W\beta_H x_W\right. \\
& \left. -4\beta_W^2) + (1+\beta_W^2-\beta_W^4)^2\right] \\
& + \frac{1}{\beta_W^2\beta_H^2}\left(l_W + \frac{2x_W}{x_W^2-1}\right)\Bigg[\beta_H(\beta_H x_W - 4\beta_W) \\
& \times(1+\beta_W^2-\beta_W^4+3x_W^2\beta_H^2) \\
& + \beta_H^2 x_W(1-\beta_W^4+13\beta_W^2) - \frac{1}{x_W}(1+\beta_W^2-\beta_W^4)^2\Bigg] \\
& + \frac{2(1+\beta_W^2)}{\beta_W\beta_H}\left[1 + \frac{\lambda_{HHH}}{(\hat{s}-M_H^2)/M_Z^2}\right] \\
& \times\left[l_W(1+\beta_W^2-\beta_W^4-2\beta_W\beta_H x_W + \beta_H^2 x_W^2)\right. \\
& \left. + 2\beta_H(x_W\beta_H - 2\beta_W)\right]\Bigg\}
\end{aligned} \quad (20)$$

with $l_W = \log[(x_W-1)/(x_W+1)]$. After folding the cross section of the subprocess with the longitudinal W_L spectra [30],

$$f_L(z) = \frac{G_F M_W^2}{2\sqrt{2}\pi^2}\frac{1-z}{z} \qquad [z = E_W/E_e] \quad (21)$$

a rough estimate of the total e^+e^- cross section can be obtained; it exceeds the exact value by about a factor 2 to 5 depending on the collider energy and the Higgs

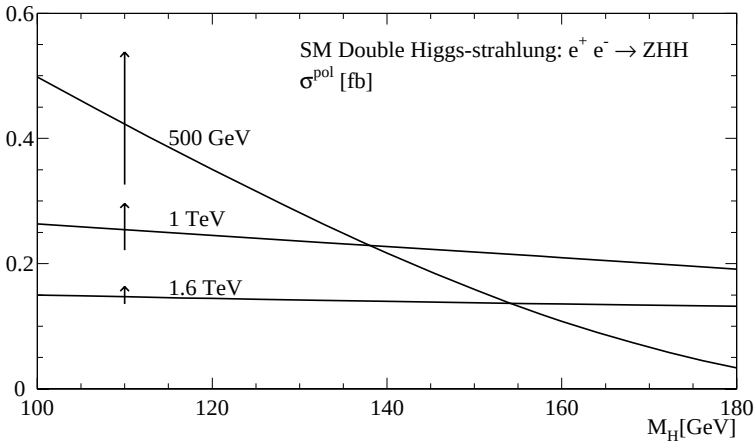

Fig. 6a. The cross section for double Higgs-strahlung in the SM at three collider energies: 500 GeV, 1 TeV and 1.6 TeV. The electron/positron beams are taken oppositely polarized. The vertical arrows correspond to a variation of the trilinear Higgs coupling from 1/2 to 3/2 of the SM value

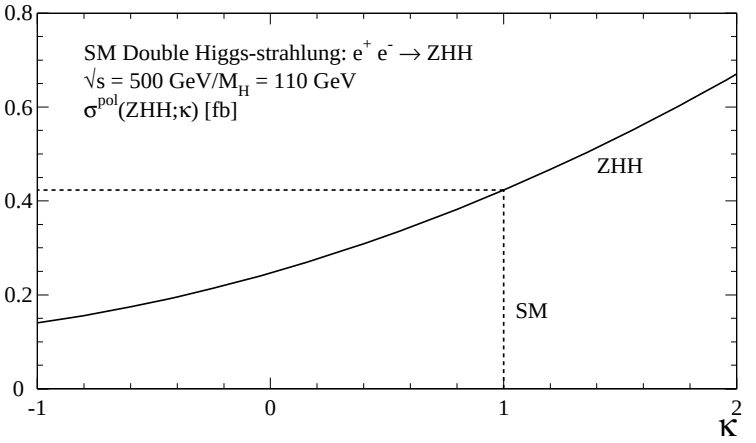

Fig. 6b. Variation of the cross section $\sigma(ZHH)$ with the modified trilinear coupling $\kappa\lambda_{HHH}$ at a collider energy of $\sqrt{s} = 500$ GeV and $M_H = 110$ GeV

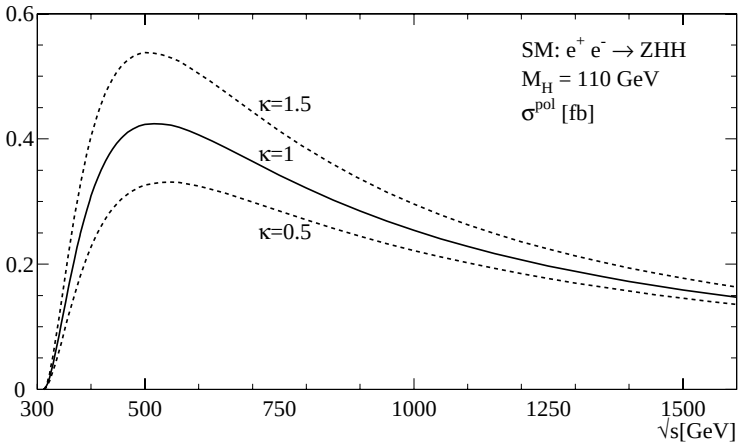

Fig. 6c. The energy dependence of the cross section for double Higgs-strahlung for a fixed Higgs mass $M_H = 110$ GeV. The variation of the cross section for modified trilinear couplings $\kappa\lambda_{HHH}$ is indicated by the dashed lines

mass. The estimate is useful nevertheless for a transparent interpretation of the exact results.

For large WW energies the process $WW \to HH$ is dominated by t-channel W exchange which is independent of the trilinear Higgs coupling. However, even at high c.m. energies the convoluted process $e^+e^- \to \bar{\nu}_e\nu_e HH$ receives most of the contributions from the lower end of the WW energy spectrum so that the sensitivity on λ_{HHH} is preserved also in this domain.

The exact cross sections for off-shell W bosons, transverse degrees of freedom included, have been calculated numerically, based on the semi-analytical CompHEP program [31]. Electron and positron beams are assumed to be polarized, giving rise to a cross section four times larger than for unpolarized beams. The results are shown in Fig. 7a for the three energies discussed before: $\sqrt{s} =$ 500 GeV, 1 TeV and 1.6 TeV. As expected, the fusion cross sections increase with rising energy. Again, the variation

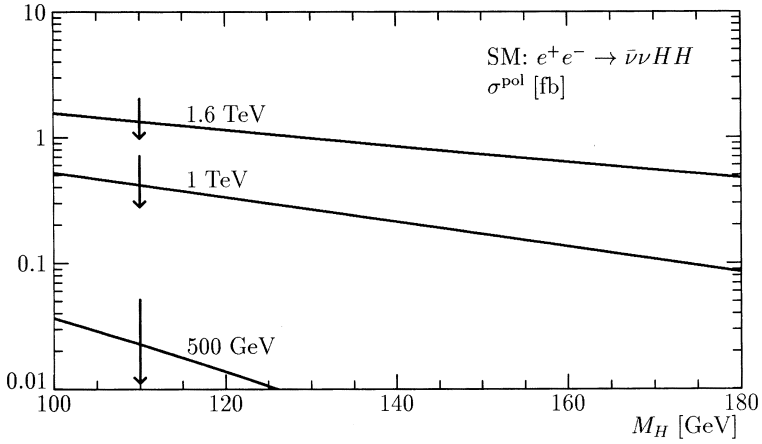

Fig. 7a. The total cross section for WW double-Higgs fusion in the SM at three collider energies: 500 GeV, 1 TeV and 1.6 TeV. The vertical arrows correspond to a variation of the trilinear Higgs coupling from 1/2 to 3/2 of the SM value

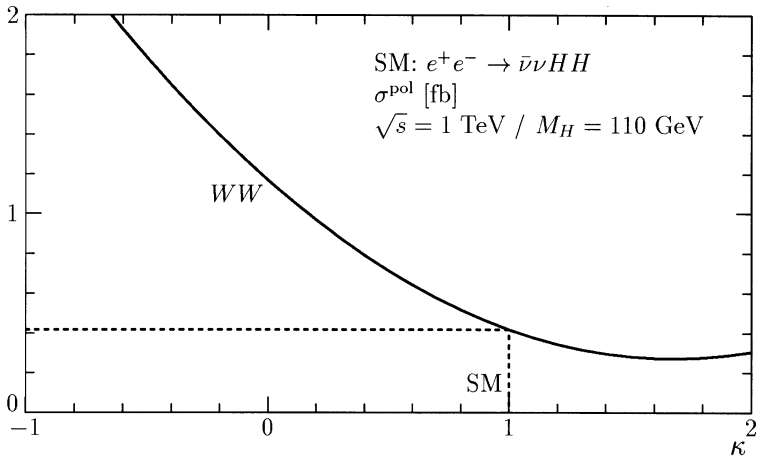

Fig. 7b. Variation of the cross section $\sigma(e^+e^- \to \bar{\nu}_e\nu_e HH)$ with the modified trilinear coupling $\kappa\lambda_{HHH}$ at a collider energy of $\sqrt{s} = 1$ TeV and $M_H = 110$ GeV

Table 2. Total cross sections for SM pair production in WW and ZZ fusion at e^+e^-colliders for two characteristic energies and masses in the intermediate range (unpolarized beams)

σ [fb]		WW	ZZ
$\sqrt{s} = 1$ TeV	$M_H = 110$ GeV	0.104	0.013
	150 GeV	0.042	0.006
	190 GeV	0.017	0.002
$\sqrt{s} = 1.6$ TeV	$M_H = 110$ GeV	0.334	0.043
	150 GeV	0.183	0.024
	190 GeV	0.103	0.013

of the cross section with $\kappa\lambda_{HHH}$, $\kappa = -1$ to $+2$, is demonstrated in Fig. 7b for $\sqrt{s} = 1$ TeV and $M_H = 110$ GeV, and by the vertical arrows for $\kappa = 1/2$ to $3/2$ in Fig. 7a. Due to the destructive interference with the gauge part of the amplitude, the cross sections drop with rising λ_{HHH}. The ZZ fusion cross section is an order of magnitude smaller than the WW fusion cross section since the Z couplings of the electron/positron are small, cf. Table 2.

It is apparent from the preceding discussion that double Higgs-strahlung $e^+e^- \to ZHH$ at moderate energies and WW fusion at TeV energies are the preferred channels for measurements of the trilinear self-coupling λ_{HHH} of the SM Higgs boson. Electron and positron beam polarization enhance the cross sections by factors 2 and 4 for Higgs-strahlung and WW fusion, respectively. Since the cross sections are small, high luminosity of the e^+e^- linear collider is essential for performing these fundamental experiments. Even though the rates of order 10^3 to $3 \cdot 10^3$ events for an integrated luminosity of 2 ab^{-1} as foreseen for TESLA are moderate, clear multi-b signatures like $e^+e^- \to Z(b\bar{b})(b\bar{b})$ and $e^+e^- \to (b\bar{b})(b\bar{b}) + \not{E}$ will help to isolate the signal from the background.

The complete reconstruction of the Higgs potential in the Standard Model requires the measurement of the quadrilinear coupling λ_{HHHH}, too. This coupling is suppressed relative to the trilinear coupling effectively by a factor of the order of the weak gauge coupling for masses in the lower part of the intermediate Higgs mass range. The quadrilinear coupling can be accessed directly only

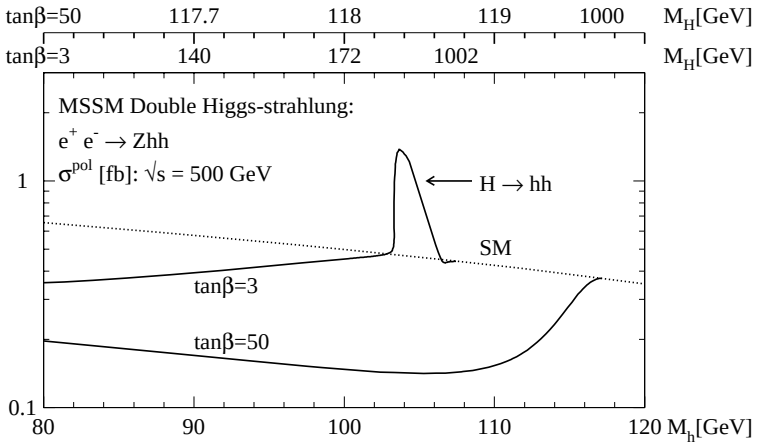

Fig. 8. Total cross sections for MSSM hh production via double Higgs-strahlung at e^+e^- linear colliders for $\tan\beta = 3$, 50 and $\sqrt{s} = 500$ GeV, including mixing effects ($A = 1$ TeV, $\mu = -1/1$ TeV for $\tan\beta = 3/50$). The dotted line indicates the SM cross section

through the production of three Higgs bosons: $e^+e^- \to ZHHH$ and $e^+e^- \to \bar{\nu}_e\nu_e HHH$. However, these cross sections are reduced by three orders of magnitude compared to the corresponding double-Higgs channels. As argued before, the signal amplitude involving the four-Higgs coupling [as well as the irreducible Higgs-strahlung amplitudes] is suppressed, leading to a reduction of the signal cross section by a factor $[\lambda^2_{HHHH}\lambda_0^4/16\pi^2]/[\lambda^2_{HHH}\lambda_0^2/M_Z^2] \sim 10^{-3}$. Irreducible background diagrams are similarly suppressed. Moreover, the phase space is reduced by the additional heavy particle in the final state. A few illustrative examples for triple Higgs-strahlung are listed in Table 3.

Table 3. Representative values for triple SM Higgs-strahlung (unpolarized beams). The sensitivity to the quadrilinear coupling is illustrated by the variation of the cross sections when λ_{HHHH} is altered by factors 1/2 and 3/2, as indicated in the square brackets

$e^+e^- \to ZHH$		σ[ab]
$\sqrt{s} = 1$ TeV	$M_H = 110$ GeV	0.44 [0.41/ 0.46]
	150 GeV	0.34 [0.32/ 0.36]
	190 GeV	0.19 [0.18/ 0.20]
$\sqrt{s} = 1.6$ TeV	$M_H = 110$ GeV	0.30 [0.29/ 0.32]
	150 GeV	0.36 [0.34/ 0.39]
	190 GeV	0.39 [0.36/ 0.43]

3 The supersymmetric Higgs sector

A large ensemble of Higgs couplings are present in supersymmetric theories. Even in the minimal realization MSSM, six different trilinear couplings hhh, Hhh, HHh, HHH, hAA, HAA are generated among the neutral particles, and many more quadrilinear couplings [22]. Since in major parts of the MSSM parameter space the Higgs bosons H, A, $H^\pm$ are quite heavy, we will focus primarily on the production of light neutral pairs hh, yet the production of heavy Higgs bosons will also be discussed where appropriate. The channels in which trilinear Higgs couplings can be probed in e^+e^- collisions, have been cataloged in Table 1.

Barring the exceptional case of very light pseudoscalar A states, λ_{Hhh} is the only trilinear coupling that may be measured in resonance decays, $H \to hh$, while all the other couplings must be accessed in continuum pair production. The relevant mechanisms have been categorized in Fig. 5 for double Higgs-strahlung, associated triple Higgs production and WW double-Higgs fusion.

3.1 Double Higgs-strahlung

The (unpolarized) cross section for double Higgs-strahlung, $e^+e^- \to Zhh$, is modified [17] (see also [19]) with regard to the Standard Model by H,A exchange diagrams,

cf. Fig. 5:

$$\frac{d\sigma(e^+e^- \to Zhh)}{dx_1 dx_2} = \frac{\sqrt{2}G_F^3 M_Z^6}{384\pi^3 s}\,\frac{v_e^2+a_e^2}{(1-\mu_Z)^2}\,\mathcal{Z}_{11} \quad (22)$$

with

$$\begin{aligned}\mathcal{Z}_{11} = {} & \mathfrak{z}^2 f_0 + \frac{\mathfrak{z}}{2}\left[\frac{\sin^2(\beta-\alpha)f_3}{y_1+\mu_{1Z}} + \frac{\cos^2(\beta-\alpha)f_3}{y_1+\mu_{1A}}\right] \\ & + \frac{\sin^4(\beta-\alpha)}{4\mu_Z(y_1+\mu_{1Z})}\left[\frac{f_1}{y_1+\mu_{1Z}} + \frac{f_2}{y_2+\mu_{1Z}}\right] \\ & + \frac{\cos^4(\beta-\alpha)}{4\mu_Z(y_1+\mu_{1A})}\left[\frac{f_1}{y_1+\mu_{1A}} + \frac{f_2}{y_2+\mu_{1A}}\right] \\ & + \frac{\sin^2 2(\beta-\alpha)}{8\mu_Z(y_1+\mu_{1A})}\left[\frac{f_1}{y_1+\mu_{1Z}} + \frac{f_2}{y_2+\mu_{1Z}}\right] \\ & + \{y_1 \leftrightarrow y_2\} \end{aligned} \quad (23)$$

and

$$\mathfrak{z} = \left[\frac{\lambda_{hhh}\sin(\beta-\alpha)}{y_3-\mu_{1Z}} + \frac{\lambda_{Hhh}\cos(\beta-\alpha)}{y_3-\mu_{2Z}}\right] + \frac{2\sin^2(\beta-\alpha)}{y_1+\mu_{1Z}} + \frac{2\sin^2(\beta-\alpha)}{y_2+\mu_{1Z}} + \frac{1}{\mu_Z} \quad (24)$$

[The notation follows the Standard Model, with $\mu_1 = M_h^2/s$ and $\mu_2 = M_H^2/s$.] In parameter ranges in which the heavy neutral Higgs boson H or the pseudoscalar Higgs boson A becomes resonant, the decay widths are implicitly included by shifting the masses to complex values $M \to M - i\Gamma/2$, *i.e.* $\mu_i \to \mu_i - i\gamma_i$ with the reduced width $\gamma_i = M_i\Gamma_i/s$, and by changing products of propagators $\pi_1\pi_2$ to $\mathrm{Re}(\pi_1\pi_2^*)$.

The total cross sections are shown in Fig. 8 for the e^+e^- collider energy $\sqrt{s} = 500$ GeV. The parameter $\tan\beta$ is chosen to be 3 and 50 and the mixing parameters $A =$ 1 TeV and $\mu = -1$ TeV and 1 TeV, respectively. If $\tan\beta$ and the mass M_h are fixed, the masses of the other heavy Higgs bosons are predicted in the MSSM [20]. Since the vertices are suppressed by $\sin/\cos$ functions of the mixing angles β and α, the continuum hh cross sections are suppressed compared to the Standard Model. The size of the cross sections increases for moderate $\tan\beta$ by nearly an order of magnitude if the hh final state can be generated in the chain $e^+e^- \to ZH \to Zhh$ via resonant H Higgs-strahlung. If the light Higgs mass approaches the upper limit for a given value of $\tan\beta$, the decoupling theorem drives the cross section of the supersymmetric Higgs boson back to its Standard Model value since the Higgs particles A, H, $H^\pm$ become asymptotically heavy in this limit. As a result of the decoupling theorem, resonance production is not effective for large $\tan\beta$. If the H mass is large enough to allow decays to hh pairs, the ZZH coupling is already too small to generate a sizable cross section.

The cross sections for other ZH_iH_j [$H_{i,j} = h$, H] final states are presented in the appendix. While the basic structure remains the same, the complexity increases due to unequal masses of the final-state particles. The reduction of the Zhh cross section is partly compensated by the ZHh and ZHH cross sections so that their sum adds up approximately to the SM value, as demonstrated in Fig. 9a for $\tan\beta = 3$ at $\sqrt{s} = 500$ GeV and hh, Hh and HH final states. Evidently, if kinematically possible, the MSSM cross sections add up to approximately the SM cross section.

3.2 Triple-Higgs production

The 2-particle processes $e^+e^- \to ZH_i$ and $e^+e^- \to AH_i$ are among themselves and mutually complementary to each other in the MSSM [32], coming with the coefficients $\sin^2(\beta-\alpha)/\cos^2(\beta-\alpha)$ and $\cos^2(\beta-\alpha)/\sin^2(\beta-\alpha)$ for $H_i = h$, H, respectively. Since multi-Higgs final states are mediated by virtual h, H bosons, the two types of self-complementarity and mutual complementarity are also operative in double-Higgs production: $e^+e^- \to ZH_iH_j$, ZAA and AH_iH_j, AAA. As the different mechanisms are intertwined, the complementarity between these 3-particle final states is of more complex matrix form, as evident from Fig. 5.

We will analyze in this section the processes involving only the light neutral Higgs boson h, $e^+e^- \to Ahh$, and three pseudoscalar Higgs bosons A, $e^+e^- \to AAA$. The more cumbersome expressions for heavy neutral Higgs bosons H are deferred to the appendix.

In the first case one finds for the unpolarized cross section

$$\frac{d\sigma[e^+e^- \to Ahh]}{dx_1dx_2} = \frac{G_F^3M_Z^6}{768\sqrt{2}\pi^3 s}\frac{v_e^2+a_e^2}{(1-\mu_Z)^2}\mathfrak{A}_{11} \quad (25)$$

where the function $\mathfrak{A}_{11}$ reads

$$\begin{aligned}\mathfrak{A}_{11} = {} & \left[\frac{c_1\lambda_{hhh}}{y_3-\mu_{1A}} + \frac{c_2\lambda_{Hhh}}{y_3-\mu_{2A}}\right]^2\frac{g_0}{2} + \frac{c_1^2\lambda_{hAA}^2}{(y_1+\mu_{1A})^2}g_1 \\ & + \frac{c_1^2d_1^2}{(y_1+\mu_{1Z})^2}g_2 \\ & + \left[\frac{c_1\lambda_{hhh}}{y_3-\mu_{1A}} + \frac{c_2\lambda_{Hhh}}{y_3-\mu_{2A}}\right]\left[\frac{c_1\lambda_{hAA}}{y_1+\mu_{1A}}g_3 + \frac{c_1d_1}{y_1+\mu_{1Z}}g_4\right] \\ & + \frac{c_1^2\lambda_{hAA}^2}{2(y_1+\mu_{1A})(y_2+\mu_{1A})}g_5 + \frac{c_1^2d_1^2}{2(y_1+\mu_{1Z})(y_2+\mu_{1Z})}g_8 \\ & + \frac{c_1^2d_1\lambda_{hAA}}{(y_1+\mu_{1A})(y_1+\mu_{1Z})}g_6 + \frac{c_1^2d_1\lambda_{hAA}}{(y_1+\mu_{1A})(y_2+\mu_{1Z})}g_7 \\ & + \{y_1 \leftrightarrow y_2\} \end{aligned} \quad (26)$$

with $\mu_{1,2} = M_{h,H}^2/s$ and the vertex coefficients

$$\begin{aligned} c_1/c_2 &= \cos(\beta-\alpha)/-\sin(\beta-\alpha) \qquad \text{and} \\ d_1/d_2 &= \sin(\beta-\alpha)/\cos(\beta-\alpha) \end{aligned} \quad (27)$$

The coefficients g_k are given by

$$\begin{aligned} g_0 &= \mu_Z[(y_1+y_2)^2 - 4\mu_A] \\ g_1 &= \mu_Z[y_1^2 - 2y_1 - 4\mu_1 + 1] \\ g_2 &= \mu_Z[y_1(y_1+2) + 4y_2(y_2+y_1-1) + 1 - 4(\mu_1+2\mu_A)] \\ &\quad +(\mu_1-\mu_A)^2[8 + [(1-y_1)^2 - 4\mu_1]/\mu_Z] \\ &\quad +(\mu_1-\mu_A)[4y_2(1+y_1) + 2(y_1^2-1)] \\ g_3 &= 2\mu_Z(y_1^2 - y_1 + y_2 + y_1y_2 - 2\mu_A) \\ g_4 &= 2\mu_Z(y_1^2 + y_1 + 2y_2^2 - y_2 + 3y_1y_2 - 6\mu_A) \\ &\quad +2(\mu_1-\mu_A)(y_1^2 - y_1 + y_2 + y_1y_2 - 2\mu_A) \\ g_5 &= 2\mu_Z(y_1 + y_2 + y_1y_2 + 4\mu_1 - 2\mu_A - 1) \\ g_6 &= 2\mu_Z(y_1^2 + 2y_1y_2 + 2y_2 + 4\mu_1 - 4\mu_A - 1) \\ &\quad +2(\mu_1-\mu_A)(y_1^2 - 2y_1 - 4\mu_1 + 1) \\ g_7 &= 2[\mu_Z(2y_1^2 - 3y_1 + y_1y_2 + y_2 - 4\mu_1 - 2\mu_A + 1) \\ &\quad +(\mu_1-\mu_A)(y_1 + y_1y_2 + y_2 + 4\mu_1 - 2\mu_A - 1)] \\ g_8 &= 2\{\mu_Z(y_1 + y_2 + 2y_1^2 + 2y_2^2 + 5y_1y_2 - 1 + 4\mu_1 \\ &\quad -10\mu_A) + 4(\mu_1-\mu_A)(-2\mu_1 - \mu_A - y_1 - y_2 + 1) \\ &\quad +[2(\mu_1-\mu_A)((y_1 + y_2 + y_1y_2 + y_1^2 + y_2^2 - 1)\mu_Z \\ &\quad +2\mu_1^2 + 4\mu_A^2 - \mu_1 + \mu_A) + 6\mu_A(\mu_A^2 - \mu_1^2) \\ &\quad +(\mu_1-\mu_A)^2(1+y_1)(1+y_2)]/\mu_Z\} \end{aligned} \quad (28)$$

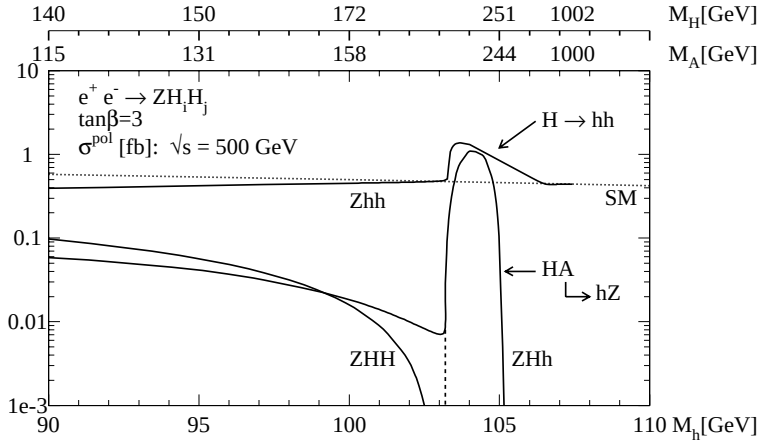

Fig. 9a. Cross sections for the processes Zhh, ZHh and ZHH for $\sqrt{s} = 500$ GeV and $\tan\beta = 3$, including mixing effects ($A = 1$ TeV, $\mu = -1$ TeV)

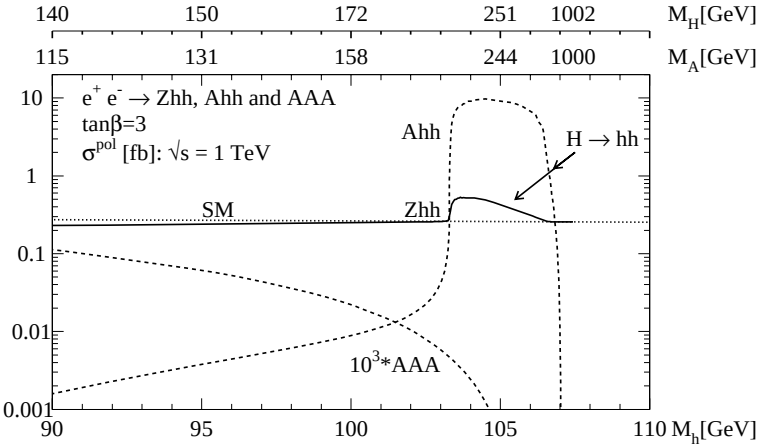

Fig. 9b. Cross sections of the processes Zhh, Ahh and AAA for $\tan\beta = 3$ and $\sqrt{s} = 1$ TeV, including mixing effects ($A = 1$ TeV, $\mu = -1$ TeV.)

The notation of the kinematics is the same as for Higgs-strahlung.

Since only a few diagrams contribute to triple A production, cf. Fig. 5, the expression for this cross section is exceptionally simple:

$$\frac{d\sigma[e^+e^- \to AAA]}{dx_1 dx_2} = \frac{G_F^3 M_Z^6}{768\sqrt{2}\pi^3 s} \frac{v_e^2 + a_e^2}{(1-\mu_Z)^2} \mathfrak{A}_{33} \quad (29)$$

where

$$\mathfrak{A}_{33} = D_3^2 g_0 + D_1^2 g_1 + D_2^2 g_1' - D_3 D_1 g_3 - D_3 D_2 g_3' + D_1 D_2 g_5 \quad (30)$$

and

$$D_k = \frac{\lambda_{hAA} c_1}{y_k - \mu_{1A}} + \frac{\lambda_{HAA} c_2}{y_k - \mu_{2A}} \quad (31)$$

The scaled mass parameter μ_1 must be replaced by μ_A in the coefficients g_i and g_i' defined earlier.

The size of the total cross section $\sigma(e^+e^- \to Ahh)$ and $\sigma(e^+e^- \to AAA)$ is compared with double Higgs-strahlung $\sigma(e^+e^- \to Zhh)$ in Fig. 9b for $\tan\beta = 3$ at $\sqrt{s} = 1$ TeV. Both these cross sections involving pseudoscalar Higgs bosons are small in the continuum. The effective coupling in the chain $Ah_{virt} \to Ahh$ is $\cos(\beta - \alpha)\lambda_{hhh}$ while in the chain $AH_{virt} \to Ahh$ it is $\sin(\beta - \alpha)\lambda_{Hhh}$; both products are small either in the first or second coefficient. Only for resonance H decays $AH \to Ahh$ the cross section becomes very large. A similar picture evolves for the triple A final state. The chain $Ah_{virt} \to AAA$ is proportional to the coefficient $\cos(\beta - \alpha)\lambda_{hAA}$ in which one of the terms is always small. The chain $AH_{virt} \to AAA$, on the other hand, is proportional to $\sin(\beta - \alpha)\lambda_{HAA}$; for this coefficient the trilinear coupling λ_{HAA} is only of order 1/2 so that, together with phase space suppression, the cross section remains small in the entire parameter space.

3.3 WW double-Higgs fusion

The WW fusion mechanism for the production of supersymmetric Higgs pairs can be treated in the same way. The dominant longitudinal amplitude for on-shell W bosons involves A, H and $H^\pm$ exchange diagrams in addition to the SM-type contributions:

$$\mathcal{M}_{LL} = \frac{G_F \hat{s}}{\sqrt{2}} \left\{ (1+\beta_W^2) \left[1 + \frac{\lambda_{hhh}\sin(\beta-\alpha)}{(\hat{s}-M_h^2)/M_Z^2} + \frac{\lambda_{Hhh}\cos(\beta-\alpha)}{(\hat{s}-M_H^2)/M_Z^2} \right] + \frac{\sin^2(\beta-\alpha)}{\beta_W \beta_h} \left[\frac{(1-\beta_W^4)+(\beta_W - \beta_h \cos\theta)^2}{\cos\theta - x_W} \right. \right.$$

$$-\frac{(1-\beta_W^4)+(\beta_W+\beta_h\cos\theta)^2}{\cos\theta+x_W}\Big]$$
$$+\frac{\cos^2(\beta-\alpha)}{\beta_W\beta_h}\left[\frac{(\beta_W-\beta_h\cos\theta)^2}{\cos\theta-x_+}-\frac{(\beta_W+\beta_h\cos\theta)^2}{\cos\theta+x_+}\right]\Big\} \quad (32)$$

As before, $\hat{s}^{1/2}$ is the c.m. energy of the subprocess, θ the scattering angle, β_W and β_h are the velocities of the W and h bosons, and

$$x_W = \frac{1-2\mu_h}{\beta_W\beta_h} \qquad \text{and}$$
$$x_+ = \frac{1-2\mu_h+2\mu_{H^\pm}-2\mu_W}{\beta_W\beta_h} \quad (33)$$

After integrating out the angular dependence, the total cross section of the fusion subprocess is given by the expression

$$\hat{\sigma}_{LL} = \frac{G_F^2M_W^4}{4\pi\hat{s}}\frac{\beta_h}{\beta_W(1-\beta_W^2)^2}\Big\{(1+\beta_W^2)^2$$
$$\times\left[\frac{\lambda_{hhh}d_1}{(\hat{s}-M_h^2)/M_Z^2}+\frac{\lambda_{Hhh}d_2}{(\hat{s}-M_H^2)/M_Z^2}+1\right]^2$$
$$+\frac{2(1+\beta_W^2)}{\beta_W\beta_h}\left[\frac{\lambda_{hhh}d_1}{(\hat{s}-M_h^2)/M_Z^2}+\frac{\lambda_{Hhh}d_2}{(\hat{s}-M_H^2)/M_Z^2}+1\right]$$
$$\times\left[d_1^2a_1^W+c_1^2a_1^+\right]+\left(\frac{d_1^2}{\beta_W\beta_h}\right)^2a_2^W+\left(\frac{c_1^2}{\beta_W\beta_h}\right)^2a_2^+$$
$$+4\left(\frac{c_1^2d_1^2}{\beta_W^2\beta_h^2}\right)[a_3^W+a_3^+]\Big\} \quad (34)$$

with

$$a_1^W = [(x_W\beta_h-\beta_W)^2+r_W]l_W+2\beta_h(x_W\beta_h-2\beta_W)$$
$$a_2^W = \left[\frac{1}{x_W}l_W+\frac{2}{x_W^2-1}\right]$$
$$\times\Big[x_W^2\beta_h^2(3\beta_h^2x_W^2+2r_W+14\beta_W^2)$$
$$-(\beta_W^2+r_W)^2-4\beta_h\beta_Wx_W(3\beta_h^2x_W^2+\beta_W^2+r_W)\Big]$$
$$-\frac{4}{x_W^2-1}\left[\beta_h^2(\beta_h^2x_W^2+4\beta_W^2-4\beta_hx_W\beta_W)\right.$$
$$\left.-(\beta_W^2+r_W)^2\right]$$
$$a_3^W = \frac{1}{x_+^2-x_W^2}\,l_W\Big[2\beta_W\beta_hx_W[(\beta_W^2+x_W^2\beta_h^2)(x_W+x_+)$$
$$+x_Wr_W+x_+r_+]-x_+(r_++r_W+\beta_h^2x_W^2)$$
$$\times(\beta_W^2+\beta_h^2x_W^2)-\beta_W^2(x_+\beta_W^2+4\beta_h^2x_W^3+x_+x_W^2\beta_h^2)$$
$$-x_+r_Wr_+\Big]+\beta_h^2\left[\beta_h^2x_+x_W\right.$$
$$\left.-2\beta_W\beta_h(x_W+x_+)+4\beta_W^2\right]$$
$$a_i^+ \equiv a_i^W \;\; (x_W\leftrightarrow x_+\;,\; r_W\leftrightarrow r_+) \quad (35)$$

and $r_W = 1-\beta_W^4$, $r_+ = 0$.

The final cross sections have been calculated for off-shell W's and transverse polarizations included, i.e. without relying on the LL and the equivalent W-boson approximation. The e^+e^- beams are assumed to be polarized. For modest $\tan\beta$, the hh continuum production is slightly suppressed by the mixing coefficients with regard to the Standard Model, Fig. 10a. The cross section is strongly enhanced in the parameter range where the fusion subprocess is resonant, $WW\to H\to hh$. For large $\tan\beta$ the WW fusion cross section is strongly suppressed by one to two orders of magnitude and resonance decay is not possible any more. This is a consequence of the small gauge couplings in this parameter range which are drastically reduced by the mixing coefficients. Since the second CP-even Higgs boson H is fairly light for these parameters, the small hh continuum production is complemented by Hh and HH production channels, as evident from Fig. 10b. The cross sections for the production of Hh, HH and AA pairs are cataloged in the appendix.

3.4 Sensitivity areas

The results obtained in the preceding sections can be summarized in compact form by constructing sensitivity areas for the trilinear SUSY Higgs couplings based on the cross sections for double Higgs-strahlung and triple Higgs production. WW double-Higgs fusion can provide additional information on the Higgs self-couplings.

The sensitivity areas will be defined in the [M_A, tanβ] plane [17]. The criteria for accepting a point in the plane as accessible for the measurement of a specific trilinear coupling are set as follows:

$$(i)\;\; \sigma[\lambda] > 0.01 \text{ fb}$$
$$(ii)\;\; \text{var}\{\lambda\to(1\pm\tfrac{1}{2})\lambda\} > 2 \text{ st.dev.}\{\lambda\} \quad (36)$$
$$\text{for} \quad \int\mathcal{L} = 2 \text{ ab}^{-1}$$

The first criterion demands at least 20 events in a sample collected for an integrated luminosity of 2 ab^{-1}, corresponding to about the lifetime of a high-luminosity machine such as TESLA. The second criterion demands a 50% change of the signal parameter to exceed a statistical fluctuation of 2 standard deviations. Even though the two criteria may look quite loose, tightening (i) and/or (ii) does not have a large impact on the size of the sensitivity areas in the [M_A, tanβ] plane, see [19]. For the sake of simplicity, the e^+e^- beams are assumed to be unpolarized and mixing effects are neglected.

Sensitivity areas of the trilinear couplings for the set of processes defined in the correlation matrix Table 1, are depicted in Figs. 11 – 13. If at most one heavy Higgs boson is present in the final states, the lower energy $\sqrt{s} = 500$ GeV is most preferable in the case of double Higgs-strahlung. HH final states in double Higgs-strahlung and triple Higgs production involving A give rise to larger sensitivity areas at the high energy $\sqrt{s} = 1$ TeV; increasing the energy to 1.6 TeV does not improve on the signal as a result of the scaling behavior of the Higgs-strahlung cross section. Apart from small regions in which interference effects play a role, the magnitude of the sensitivity regions in the parameter tanβ is readily explained by the magnitude of the

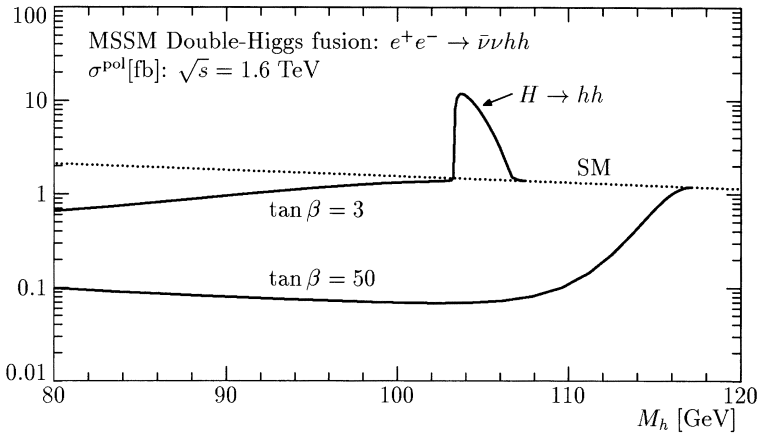

Fig. 10a. Total cross sections for MSSM hh production via double WW double-Higgs fusion at e^+e^- linear colliders for $\tan\beta = 3$, 50 and $\sqrt{s} = 1.6$ TeV, including mixing effects ($A = 1$ TeV, $\mu = -1/1$ TeV for $\tan\beta = 3/50$)

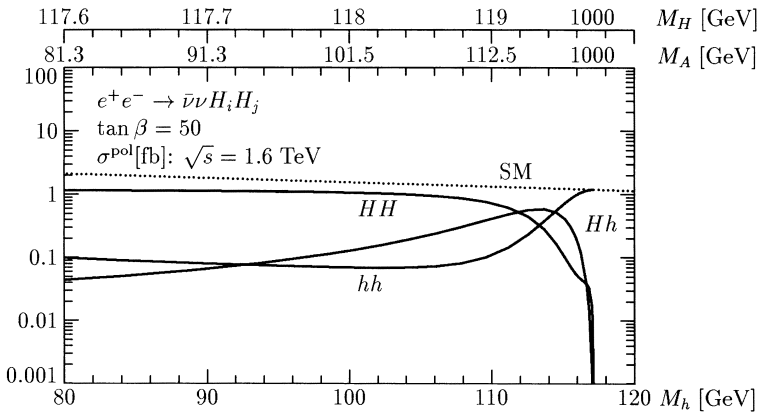

Fig. 10b. Total cross sections for WW double-Higgs fusion with hh, Hh and HH final states for $\sqrt{s} = 1.6$ TeV and $\tan\beta = 50$, including mixing effects ($A = 1$ TeV, $\mu = 1$ TeV)

parameters $\lambda \sin(\beta - \alpha)$ and $\lambda \cos(\beta - \alpha)$, shown individually in Figs. 2 and 3. For large M_A the sensitivity criteria cannot be met any more either as a result of phase space effects or due to the suppression of the H, A, $H^\pm$ propagators for large masses. While the trilinear coupling of the light neutral CP-even Higgs boson is accessible in nearly the entire MSSM parameter space, the regions for λ's involving heavy Higgs bosons are rather restricted.

Since neither experimental efficiencies nor background related cuts are considered in this paper, the areas shown in Figs. 11, 12 and 13 must be interpreted as maximal envelopes. They are expected to shrink when experimental efficiencies are properly taken into account; more elaborate cuts on signal and backgrounds, however, may help reduce their impact.

4 Conclusions

In the present paper we have analyzed the production of Higgs boson pairs and triple Higgs final states at e^+e^- linear colliders. They will allow us to measure fundamental trilinear Higgs self-couplings. The first theoretical steps into this area have been taken by calculating the production cross sections in the Standard Model for Higgs bosons in the intermediate mass range and for Higgs bosons in the minimal supersymmetric extension. Earlier results have been combined with new calculations in this analysis.

The cross sections in the Standard Model for double Higgs-strahlung, triple Higgs production and double-Higgs fusion are small so that high luminosities are needed to perform these experiments. Even though the e^+e^- cross sections are below the hadronic cross sections, the strongly reduced number of background events renders the search for the Higgs-pair signal events, through $bbbb$ final states for instance, easier in the e^+e^- environment than in jetty LHC final states. For sufficiently high luminosities even the first phase of these colliders with an energy of 500 GeV will allow the experimental analysis of self-couplings for Higgs bosons in the intermediate mass range.

The extended Higgs spectrum in supersymmetric theories gives rise to a plethora of trilinear and quadrilinear couplings. The hhh coupling is generally quite different from the Standard Model. It can be measured in hh continuum production at e^+e^- linear colliders. Other couplings between heavy and light MSSM Higgs bosons can be measured as well, though only in restricted areas of the [M_A, $\tan\beta$] parameter space as illustrated in the set of Figs. 11 – 13.

Acknowledgements. W.K. has been supported by the German Bundesministerium für Bildung und Forschung (BMBF), Contract Nr. 05 6HD 91 P(0). We gratefully acknowledge discussions with M. Drees, M. Dubinin, H. Haber, P. Lutz, L. Ma-

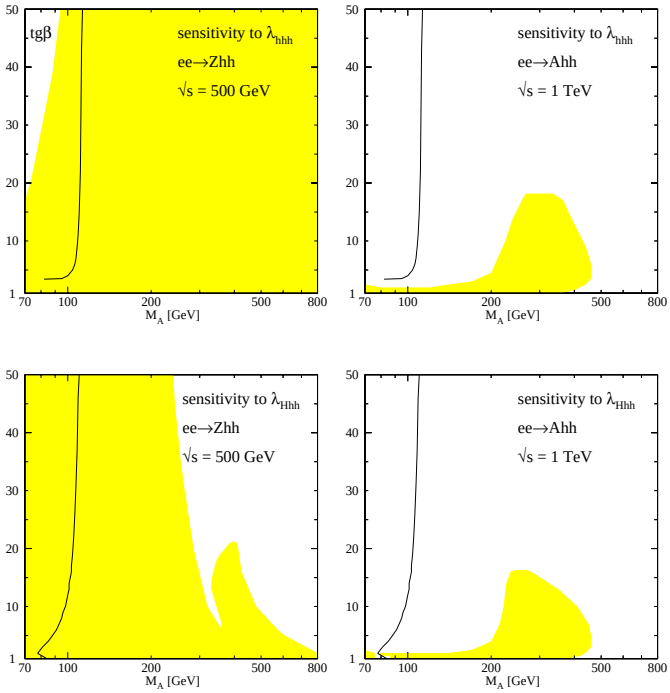

Fig. 11. Sensitivity to λ_{hhh} and λ_{Hhh} in the processes $e^+e^- \to Zhh$ and $e^+e^- \to Ahh$ for collider energies 500 GeV and 1 TeV, respectively (no mixing). [Vanishing trilinear couplings are indicated by contour lines.]

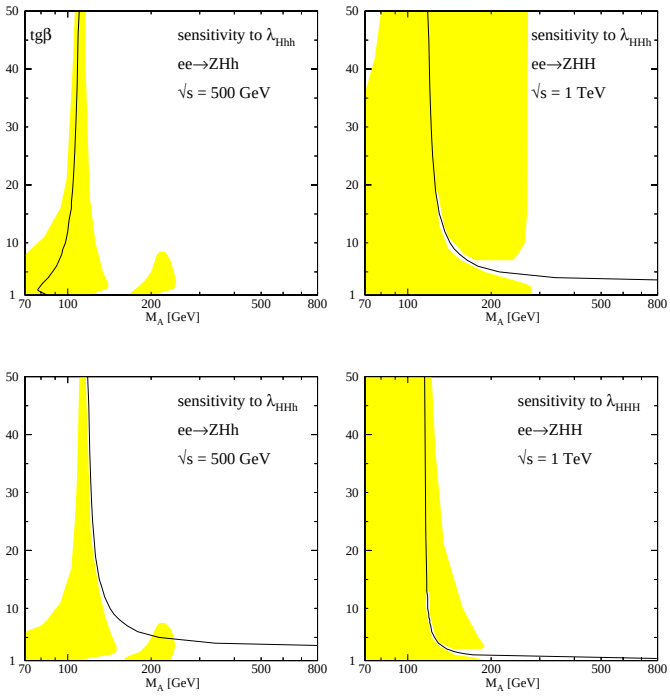

Fig. 12. Sensitivity to λ_{Hhh}, λ_{HHh} and λ_{HHH} in the processes $e^+e^- \to ZHh$ and $e^+e^- \to ZHH$ for collider energies 500 GeV and 1 TeV, respectively (no mixing)

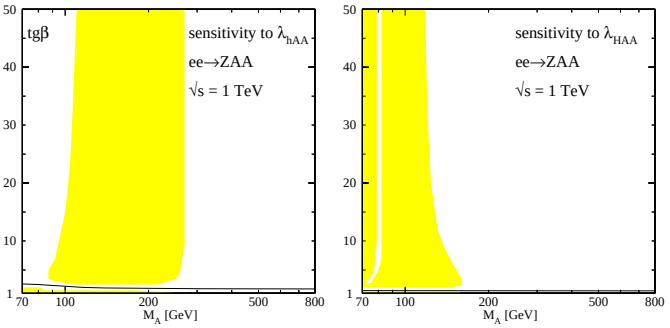

Fig. 13. Sensitivity to λ_{hAA} and λ_{HAA} in the process $e^+e^- \to ZAA$ for a collider energy of 1 TeV (no mixing)

iani, P. Osland, P. Pandita, F. Richard and R. Settles. Special thanks go to M. Spira for providing us with a program for 2-loop SUSY couplings, and for the careful reading of the manuscript.

Appendix A: Double Higgs-strahlung processes

In this appendix, we present the cross sections for the pair production of the heavy MSSM Higgs bosons in the Higgs-strahlung processes, $e^+e^- \to ZH_iH_j$ and ZAA with $H_{i,j} = h, H$. The mixed process $e^+e^- \to ZH_iA$ is generated at the tree level by gauge couplings only. The notation is the same as in Sect. 2.1. The trilinear couplings have been introduced earlier. Modifications of the SM Higgs-gauge coupling in the MSSM are accounted for by the mixing parameters:

$$\begin{array}{lll} VVh: & d_1 = \sin(\beta-\alpha) & VVH: \ d_2 = \cos(\beta-\alpha) \\ VVA: & d_3 = 0 & \\ VAh: & c_1 = \cos(\beta-\alpha) & VAH: \ c_2 = -\sin(\beta-\alpha) \\ WAH: & c_3 = 1 & \end{array} \quad \text{(A.1)}$$

for $V = Z$ and W. The Higgs bosons are neutral except in the last entry.

A1: $e^+e^- \to ZH_iH_j$

The double differential cross section of the process $e^+e^- \to ZH_iH_j$ is given for unpolarized beams by the expression

$$\frac{d\sigma[e^+e^- \to ZH_iH_j]}{dx_1 dx_2} = \frac{\sqrt{2}\, G_F^3\, M_Z^6}{384\,\pi^3 s} \frac{v_e^2 + a_e^2}{(1-\mu_Z)^2}\ \mathcal{Z}_{ij} \quad \text{(A.2)}$$

In terms of the variables y_1, y_2, y_3 defined in Sect. 2.1, and with $\mu_i = M_{H_i}^2/s$, $\mu_{ij} = \mu_i - \mu_j$, etc., the coefficient $\mathcal{Z}_{ij}$ in the cross sections can be written as

$$\mathcal{Z}_{ij} = \mathfrak{z}_{ij}^2 f_0 + \frac{\mathfrak{z}_{ij}}{2}\left[\frac{d_i d_j f_3}{y_1+\mu_{iZ}} + \frac{c_i c_j f_3}{y_1+\mu_{iA}}\right] + \frac{(d_i d_j)^2}{4\mu_Z(y_1+\mu_{iZ})}\left[\frac{f_1}{y_1+\mu_{iZ}} + \frac{f_2}{y_2+\mu_{jZ}}\right] + \frac{(c_i c_j)^2}{4\mu_Z(y_1+\mu_{iA})}\left[\frac{f_1}{y_1+\mu_{iA}} + \frac{f_2}{y_2+\mu_{jA}}\right] + \frac{d_i d_j c_i c_j}{2\mu_Z(y_1+\mu_{iA})}\left[\frac{f_1}{y_1+\mu_{iZ}} + \frac{f_2}{y_2+\mu_{jZ}}\right] + \left\{(y_1,\mu_i)\leftrightarrow(y_2,\mu_j)\right\} \quad (A.3)$$

with

$$\mathfrak{z}_{ij} = \left[\frac{d_1\lambda_{hH_iH_j}}{y_3-\mu_{1Z}} + \frac{d_2\lambda_{HH_iH_j}}{y_3-\mu_{2Z}}\right] + \frac{2d_id_j}{y_1+\mu_{iZ}} + \frac{2d_id_j}{y_2+\mu_{jZ}} + \frac{\delta_{ij}}{\mu_Z} \quad (A.4)$$

The coefficients f_0 to f_3 are given by

$$\begin{aligned}
f_0 &= \mu_Z[(y_1+y_2)^2+8\mu_Z]/8\\
f_1 &= (y_1-1)^2(\mu_Z-y_1)^2 - 4\mu_i y_1(y_1+y_1\mu_Z-4\mu_Z)\\
&\quad +\mu_Z(\mu_Z-4\mu_i)(1-4\mu_i)-\mu_Z^2\\
&\quad +(\mu_i-\mu_j)^2[y_1(y_1-2)+1-4\mu_i]\\
&\quad +(\mu_i-\mu_j)[8\mu_i(-y_1-\mu_Z)+2y_1\mu_Z(y_1-2)+2\mu_Z\\
&\quad +2y_1(y_1-1)^2]\\
f_2 &= [\mu_Z(1+\mu_Z-y_1-y_2-8\mu_i)\\
&\quad -(1+\mu_Z)y_1y_2](2+2\mu_Z-y_1-y_2)\\
&\quad +y_1y_2[y_1y_2+\mu_Z^2+1+4\mu_i(1+\mu_Z)]\\
&\quad +4\mu_i\mu_Z(1+\mu_Z+4\mu_i)+\mu_Z^2\\
&\quad -2(\mu_i-\mu_j)^3-(\mu_i-\mu_j)^2[y_2(y_1-1)\\
&\quad +10\mu_Z+4\mu_j+3y_1-1]\\
&\quad +(\mu_i-\mu_j)[\mu_Z(2(-y_1y_2-y_1-8\mu_j)\\
&\quad +6(\mu_Z+1-y_2))+y_1((y_2-1)^2\\
&\quad -y_1(1+y_2))+y_2(y_2-1)-4\mu_j(y_1-y_2)]\\
f_3 &= y_1(y_1-1)(\mu_Z-y_1)-y_2(y_1+1)(y_1+\mu_Z)\\
&\quad +2\mu_Z(\mu_Z+1-4\mu_i)\\
&\quad +2(\mu_i-\mu_j)^2-(\mu_i-\mu_j)\\
&\quad \times[y_2+y_1^2-3y_1+y_1y_2-4\mu_Z]
\end{aligned} \quad (A.5)$$

For resonance contributions, propagator products have to be substituted by $\pi_1(\mu_i)\pi_2(\mu_j) \to Re\,\{\pi_1(\mu_i)\pi_2(\mu_j^*)\}$ with $\mu_i \to \mu_i - i\gamma_i$ and $\gamma_i = M_{H_i}\Gamma_{H_i}/s$. Setting $i=j=1$, one recovers the expressions (22–24) for the process $e^+e^- \to Zhh$.

A2: $e^+e^- \to ZAA$

The differential cross section of the process $e^+e^- \to ZAA$ is given by inserting $\mathcal{Z}_{33}$ in (A.2):

$$\mathcal{Z}_{33} = \mathfrak{z}_{33}^2 f_0 + \tfrac{\mathfrak{z}_{33}}{2}\left[\tfrac{c_1^2}{y_1-\mu_{1A}}+\tfrac{c_2^2}{y_1-\mu_{2A}}\right]f_3 + \tfrac{1}{4\mu_Z}\left[\tfrac{c_1^2}{y_1-\mu_{1A}}+\tfrac{c_2^2}{y_1-\mu_{2A}}\right]\left[\tfrac{c_1^2}{y_2-\mu_{1A}}+\tfrac{c_2^2}{y_2-\mu_{2A}}\right]f_2 + \tfrac{1}{4\mu_Z}\left[\tfrac{c_1^2}{y_1-\mu_{1A}}+\tfrac{c_2^2}{y_1-\mu_{2A}}\right]^2 f_1 + \{y_1\leftrightarrow y_2\} \quad (A.6)$$

where

$$\mathfrak{z}_{33} = \left[\frac{d_1\lambda_{hAA}}{y_3-\mu_{1Z}} + \frac{d_2\lambda_{HAA}}{y_3-\mu_{2Z}}\right] + \frac{1}{\mu_Z} \quad (A.7)$$

The coefficients f_0 to f_3 follow from the previous subsection after substituting μ_1, $\mu_2 \to \mu_A$.

Appendix B: Triple Higgs boson production

The cross sections for the triple Higgs boson production of MSSM Higgs bosons, $e^+e^- \to AH_iH_j$ and $e^+e^- \to AAA$ with $H_{i,j} = h, H$ are presented in this second appendix. The remaining process $e^+e^- \to H_iAA$ does not occur at tree level because of CP–invariance.

B1: $e^+e^- \to AH_iH_j$

The double differential cross section of the process $e^+e^- \to AH_iH_j$ for unpolarized beams reads in the same notation as above:

$$\frac{d\sigma}{dx_1dx_2} = \frac{G_F^3M_Z^6}{768\sqrt{2}\pi^3 s}\,\frac{v_e^2+a_e^2}{(1-\mu_Z)^2}\,\mathfrak{A}_{ij} \quad (B.1)$$

with the function $\mathfrak{A}_{ij}$

$$\begin{aligned}
\mathfrak{A}_{ij} &= \left[\frac{\lambda_{hH_iH_j}c_1}{y_3-\mu_{1A}} + \frac{\lambda_{HH_iH_j}c_2}{y_3-\mu_{2A}}\right]^2 g_0 + \frac{\lambda_{H_jAA}^2c_i^2}{(y_1+\mu_{iA})^2}g_1\\
&\quad + \frac{\lambda_{H_iAA}^2c_j^2}{(y_2+\mu_{jA})^2}g_1' + \frac{c_j^2d_i^2}{(y_1+\mu_{iZ})^2}g_2 + \frac{c_i^2d_j^2}{(y_2+\mu_{jZ})^2}g_2'\\
&\quad + \left[\frac{\lambda_{hH_iH_j}c_1}{y_3-\mu_{1A}} + \frac{\lambda_{HH_iH_j}c_2}{y_3-\mu_{2A}}\right]\left[\frac{\lambda_{H_jAA}c_i}{y_1+\mu_{iA}}g_3 + \frac{\lambda_{H_iAA}c_j}{y_2+\mu_{jA}}g_3'\right.\\
&\quad \left. + \frac{c_jd_i}{y_1+\mu_{iZ}}g_4 + \frac{c_id_j}{y_2+\mu_{jZ}}g_4'\right]\\
&\quad + \frac{\lambda_{H_iAA}\lambda_{H_jAA}c_ic_j}{(y_1+\mu_{iA})(y_2+\mu_{jA})}g_5 + \frac{c_ic_jd_id_j}{(y_1+\mu_{iZ})(y_2+\mu_{jZ})}g_8\\
&\quad + \frac{\lambda_{H_jAA}c_ic_jd_i}{(y_1+\mu_{iA})(y_1+\mu_{iZ})}g_6 + \frac{\lambda_{H_iAA}c_ic_jd_j}{(y_2+\mu_{jA})(y_2+\mu_{jZ})}g_6'\\
&\quad + \frac{\lambda_{H_jAA}c_i^2d_j}{(y_1+\mu_{iA})(y_2+\mu_{jZ})}g_7 + \frac{\lambda_{H_iAA}c_j^2d_i}{(y_2+\mu_{jA})(y_1+\mu_{iZ})}g_7'
\end{aligned} \quad (B.2)$$

The following expressions must be inserted for the coefficients g_k:

$$\begin{aligned}
g_0 &= \mu_Z[(y_1+y_2)^2-4\mu_A]\\
g_1 &= \mu_Z(y_1^2-2y_1-4\mu_i+1)\\
g_2 &= \mu_Z(2y_1+y_1^2-4y_2+4y_2^2+4y_1y_2+1\\
&\quad +4\mu_i-8\mu_j-8\mu_A)+(\mu_j-\mu_A)^2
\end{aligned}$$

$$
\begin{aligned}
&[8+(-2y_1+y_1^2-4\mu_i+1)/\mu_Z]\\
&+2(\mu_j-\mu_A)(2y_1y_2+y_1^2+2y_2-1)\\
g_3 &= 2\mu_Z(y_1^2+y_1y_2-y_1+y_2+2\mu_j-2\mu_i-2\mu_A)\\
g_4 &= 2\mu_Z(y_1-y_2+y_1^2+2y_2^2+3y_1y_2-2\mu_j+2\mu_i-6\mu_A)\\
&+2(\mu_j-\mu_A)(-y_1+y_2+y_1^2+y_1y_2\\
&+2\mu_j-2\mu_A-2\mu_i)\\
g_5 &= 2\mu_Z(y_1+y_2+y_1y_2+2\mu_j+2\mu_i-2\mu_A-1)\\
g_6 &= 2\mu_Z(y_1^2+2y_1y_2+2y_2+4\mu_j-4\mu_A-1)\\
&+2(\mu_j-\mu_A)(y_1^2-2y_1-4\mu_i+1)\\
g_7 &= 2[\mu_Z(2y_1^2+y_1y_2+y_2-3y_1+2\mu_j-6\mu_i-2\mu_A+1)\\
&+(\mu_i-\mu_A)(y_1+y_2+y_1y_2+2\mu_j+2\mu_i-2\mu_A-1)]\\
g_8 &= 2\{\mu_Z(y_1+y_2+2y_1^2+2y_2^2+5y_1y_2-1+2\mu_j+2\mu_i\\
&-10\mu_A)+2(\mu_i-\mu_A)(\mu_i-3\mu_j-\mu_A-2y_2+1)\\
&+2(\mu_j-\mu_A)(\mu_j-3\mu_i-\mu_A-2y_1+1)\\
&+[(\mu_j-\mu_A)((1+y_1)(y_2+2y_1-1)\mu_Z\\
&+2\mu_i^2+4\mu_A^2+\mu_A-\mu_i)\\
&+(\mu_i-\mu_A)((1+y_2)(y_1+2y_2-1)\mu_Z\\
&+2\mu_j^2+4\mu_A^2+\mu_A-\mu_j)\\
&+6\mu_A(\mu_A^2-\mu_i\mu_j)+(\mu_i-\mu_A)\\
&\times(\mu_j-\mu_A)(1+y_1)(1+y_2)]/\mu_Z\}
\end{aligned}
\tag{B.3}
$$

and

$$
g_k'(y_1,y_2,\mu_i,\mu_j)=g_k(y_2,y_1,\mu_j,\mu_i) \tag{B.4}
$$

Appendix C: Heavy Higgs production in W_LW_L fusion

In this third appendix we list the amplitudes and cross sections for the pair production of the CP–even Higgs bosons in the longitudinal W approximation $W_LW_L \to H_iH_j$, as well as for $W_LW_L \to AA$. The notation is the same as in Sect. 2.2.

C1: $W_LW_L \to H_iH_j$

The amplitudes for the process $W_LW_L \to H_iH_j$ are given by:

$$
\begin{aligned}
\mathcal{M}_{LL} = \tfrac{G_F\hat{s}}{\sqrt{2}}\Big\{&(1+\beta_W^2)\left[\delta_{ij}+\tfrac{\lambda_{hH_iH_j}d_1}{(\hat{s}-M_h^2)/M_Z^2}+\tfrac{\lambda_{HH_iH_j}d_2}{(\hat{s}-M_H^2)/M_Z^2}\right]\\
&+\tfrac{d_id_j}{\beta_W\lambda_{ij}}\left[\tfrac{r_W+(\beta_W-\lambda_{ij}\cos\theta)^2}{\cos\theta-x_W}-\tfrac{r_W+(\beta_W+\lambda_{ij}\cos\theta)^2}{\cos\theta+x_W}\right]\\
&+\tfrac{c_ic_j}{\beta_W\lambda_{ij}}\left[\tfrac{r_++(\beta_W-\lambda_{ij}\cos\theta)^2}{\cos\theta-x_+}-\tfrac{r_++(\beta_W+\lambda_{ij}\cos\theta)^2}{\cos\theta+x_+}\right]\Big\}
\end{aligned}
\tag{C.1}
$$

where $\mu_{i,j}=M^2_{H_{i,j}}/\hat{s}$, $\beta_W=(1-4M_W^2/\hat{s})^{1/2}$ and λ_{ij} is the usual two–body phase space function, $\lambda_{ij}^2=(1-\mu_i-\mu_j)^2-4\mu_i\mu_j$. Furthermore,

$$
\begin{aligned}
x_W &= (1-\mu_i-\mu_j)/(\beta_W\lambda_{ij})\\
r_W &= 1-\beta_W^4-\beta_W^2(\mu_i-\mu_j)^2\\
x_+ &= (1-\mu_i-\mu_j+2M^2_{H^\pm}/\hat{s}-2M_W^2/\hat{s})/(\beta_W\lambda_{ij})\\
r_+ &= -\beta_W^2(\mu_i-\mu_j)^2
\end{aligned}
\tag{C.2}
$$

The total cross section of the subprocess is obtained by integrating the squared amplitude over the scattering angle; the result may be written:

$$
\begin{aligned}
&\sigma_{LL}(H_iH_j)=\tfrac{1}{1+\delta_{ij}}\tfrac{G_F^2M_W^4}{2\pi\hat{s}}\tfrac{\lambda_{ij}}{\beta_W(1-\beta_W^2)^2}\\
&\Big\{(1+\beta_W^2)^2\left[\delta_{ij}+\tfrac{\lambda_{hH_iH_j}d_1}{(\hat{s}-M_h^2)/M_Z^2}+\tfrac{\lambda_{HH_iH_j}d_2}{(\hat{s}-M_H^2)/M_Z^2}\right]^2\\
&+\tfrac{2(1+\beta_W^2)}{\beta_W\lambda_{ij}}\left[\delta_{ij}+\tfrac{\lambda_{hH_iH_j}d_1}{(\hat{s}-M_h^2)/M_Z^2}+\tfrac{\lambda_{HH_iH_j}d_2}{(\hat{s}-M_H^2)/M_Z^2}\right]\\
&\times\left[d_id_ja_1^W+c_ic_ja_1^+\right]\\
&+\left(\tfrac{d_id_j}{\beta_W\lambda_{ij}}\right)^2a_2^W+\left(\tfrac{c_ic_j}{\beta_W\lambda_{ij}}\right)^2a_2^+ +4\left(\tfrac{d_id_jc_ic_j}{\beta_W^2\lambda_{ij}^2}\right)[a_3^W+a_3^+]\Big\}
\end{aligned}
\tag{C.3}
$$

with

$$
\begin{aligned}
a_1^W &= [(x_W\lambda_{ij}-\beta_W)^2+r_W]\log\frac{x_W-1}{x_W+1}\\
&+2\lambda_{ij}(x_W\lambda_{ij}-2\beta_W)\\
a_2^W &= \left[\frac{1}{x_W}\log\frac{x_W-1}{x_W+1}+\frac{2}{x_W^2-1}\right]\\
&\times\Big[x_W^2\lambda_{ij}^2(3\lambda_{ij}^2x_W^2+2r_W+14\beta_W^2)\\
&-(\beta_W^2+r_W)^2-4\lambda_{ij}\beta_Wx_W(3\lambda_{ij}^2x_W^2+\beta_W^2+r_W)\Big]\\
&-\frac{4}{x_W^2-1}\left[\lambda_{ij}^2(\lambda_{ij}^2x_W^2+4\beta_W^2-4\lambda_{ij}x_W\beta_W)\right.\\
&\left.-(\beta_W^2+r_W)^2\right]\\
a_3^W &= \frac{1}{x_+^2-x_W^2}\log\frac{x_W-1}{x_W+1}\Big[2\beta_W\lambda_{ij}x_W[(\beta_W^2+x_W^2\lambda_{ij}^2)\\
&\times(x_W+x_+)+x_Wr_W+x_+r_+]\\
&-x_+(r_++r_W+\lambda_{ij}^2x_W^2)(\beta_W^2+\lambda_{ij}^2x_W^2)\\
&-\beta_W^2(x_+\beta_W^2+4\lambda_{ij}^2x_W^3+x_+x_W^2\lambda_{ij}^2)-x_+r_Wr_+\Big]\\
&+\lambda_{ij}^2\left[\lambda_{ij}^2x_+x_W-2\beta_W\lambda_{ij}(x_W+x_+)+4\beta_W^2\right]
\end{aligned}
$$

$$
a_i^+ \equiv a_i^W \ (x_W\leftrightarrow x_+\ ,\ r_W\leftrightarrow r_+) \tag{C.4}
$$

C2: $W_LW_L \to AA$

For pseudoscalar Higgs bosons, amplitude and cross section are significantly simpler since only a few diagrams contribute to the AA final state and, moreover, the masses of the final-state particles are equal:

$$
\begin{aligned}
\mathcal{M}_{LL} = \tfrac{G_F\hat{s}}{\sqrt{2}}\Big\{&(1+\beta_W^2)\left[1+\tfrac{\lambda_{hAA}d_1}{(\hat{s}-M_h^2)/M_Z^2}+\tfrac{\lambda_{HAA}d_2}{(\hat{s}-M_H^2)/M_Z^2}\right]\\
&+\tfrac{1}{\beta_W\beta_A}\left[\tfrac{(\beta_W-\beta_A\cos\theta)^2}{\cos\theta-x_A}-\tfrac{(\beta_W+\beta_A\cos\theta)^2}{\cos\theta+x_A}\right]\Big\}
\end{aligned}
\tag{C.5}
$$

with

$$\beta_A = (1-4M_A^2/\hat{s})^{1/2} \quad \text{and}$$
$$x_A = (1-2M_A^2/\hat{s}+2M_{H^\pm}^2/\hat{s}-2M_W^2/\hat{s})/(\beta_W\beta_A) \quad \text{(C.6)}$$

The total cross section for the subprocess $W_LW_L \to AA$ may be cast into the form

$$\begin{aligned}
\sigma_{LL}(AA) = {} & \tfrac{G_F^2 M_W^4}{4\pi\hat{s}} \tfrac{\beta_A}{\beta_W(1-\beta_W^2)^2} \Bigg\{ (1+\beta_W^2)^2 \\
& \times \left[1 + \tfrac{\lambda_{hAA}d_1}{(\hat{s}-M_h^2)/M_Z^2} + \tfrac{\lambda_{HAA}d_2}{(\hat{s}-M_H^2)/M_Z^2}\right]^2 \\
& +2(1+\beta_W^2)\left[1 + \tfrac{\lambda_{hAA}d_1}{(\hat{s}-M_h^2)/M_Z^2} \; + \; \tfrac{\lambda_{HAA}d_2}{(\hat{s}-M_H^2)/M_Z^2}\right] \\
& \times \tfrac{1}{\beta_W\beta_A}\left[(x_A\beta_A-\beta_W)^2 \log\tfrac{x_A-1}{x_A+1} + 2\beta_A(x_A\beta_A-2\beta_W)\right] \\
& + \tfrac{1}{\beta_A^2\beta_W^2}\Bigg(\log\tfrac{x_A-1}{x_A+1}\left[3\beta_A^2 x_A(\beta_A x_A-2\beta_W)^2\right. \\
& \left. +\beta_W^2(2\beta_A^2 x_A - 4\beta_W\beta_A - \beta_W^2/x_A)\right] \\
& + \tfrac{2}{x_A^2-1}\left[(3x_A^2\beta_A^2 - 2\beta_A^2 + \beta_W^2)(\beta_A x_A - 2\beta_W)^2\right. \\
& \left. +\beta_W^2(\beta_A^2 x_A^2 - 3\beta_W^2)\right]\Bigg)\Bigg\} \qquad \text{(C.7)}
\end{aligned}$$

C3: Asymptotia

For asymptotic energies, the leading part of the WW cross sections does not involve the trilinear couplings $H_iH_jH_k$ or H_iH_jA. Note however that the convoluted leptonic cross sections $e^+e^- \longrightarrow \bar{\nu}_e\nu_e H_iH_j$ and AA are dominated by the threshold regions, also for asymptotic e^+e^- energies, so that the observable leptonic high-energy cross sections are indeed sensitive in leading order to the trilinear Higgs couplings.

References

1. P.W. Higgs, Phys. Lett. **12** (1964) 132; Phys. Rev. **145** (1966) 1156; F. Englert, R. Brout, Phys. Rev. Lett. **13** (1964) 321; G.S. Guralnik, C.R. Hagen, T.W. Kibble, Phys. Rev. Lett. **13** (1964) 585
2. For a review see: J.F. Gunion, H.E. Haber, G. Kane, S. Dawson, *The Higgs Hunter's Guide*, Addison-Wesley, 1990
3. G. Gounaris, D. Schildknecht, F. Renard, Phys. Lett. B **83** (1979) 191, (**E**) **89B** (1980) 437; V. Barger, T. Han, R.J.N. Phillips, Phys. Rev. D **38** (1988) 2766
4. V.A. Ilyin, A.E. Pukhov, Y. Kurihara, Y. Shimizu, T. Kaneko, Phys. Rev. D **54** (1996) 6717
5. F. Boudjema, E. Chopin, Z. Phys. C **73** (1996) 85
6. V. Barger, T. Han, Mod. Phys. Lett. A **5** (1990) 667
7. A. Dobrovolskaya, V. Novikov, Z. Phys. C **52** (1991) 427
8. D.A. Dicus, K.J. Kallianpur, S.S.D. Willenbrock, Phys. Lett. B **200** (1988) 187; A. Abbasabadi, W.W. Repko, D.A. Dicus, R. Vega, Phys. Rev. D **38** (1988) 2770; Phys. Lett. B **213** (1988) 386
9. E.W.N. Glover, J.J. van der Bij, Nucl. Phys. B **309** (1988) 282
10. T. Plehn, M. Spira, P.M. Zerwas, Nucl. Phys. B **479** (1996) 46; (E) Nucl. Phys. B **531** (1998) 655
11. S. Dawson, S. Dittmaier, M. Spira, Phys. Rev. D **58** (1998) 115012
12. G. Jikia, Nucl. Phys. B **412** (1994) 57
13. J.F. Gunion, H.E. Haber, Nucl. Phys. B **272** (1986) 1; B **278** (1986) 449
14. H.E. Haber, R. Hempfling, Phys. Rev. Lett. **66** (1991) 1815; Y. Okada, M. Yamaguchi, T. Yanagida, Prog. Theor. Phys. **85** (1991) 1; J. Ellis, G. Ridolfi, F. Zwirner, Phys. Lett. B **257** (1991) 83
15. M. Carena, J.R. Espinosa, M. Quiros, C.E.M. Wagner, Phys. Lett. B **335** (1995) 209; M. Carena, M. Quiros, C.E.M. Wagner, Nucl. Phys. B **461** (1996) 407; H.E. Haber, R. Hempfling, A.H. Hoang, Z. Phys. C **75** (1997) 539; S. Heinemeyer, W. Hollik, G. Weiglein, KA-TP-17-1998 [hep-ph/9812472]
16. A. Djouadi, J. Kalinowski, M. Spira, Comput. Phys. Comm. **108** (1998) 56; M. Spira, private communication
17. A. Djouadi, H.E. Haber, P.M. Zerwas, Phys. Lett. B **375** (1996) 203 and (E) in press
18. M. Carena, P.M. Zerwas, Proceedings, Physics at LEP2, CERN 96-01 [hep-ph/9602250]
19. P. Osland, P.N. Pandita, Phys. Rev. D **59** (1999) 055013
20. A. Djouadi, J. Kalinowski, P.M. Zerwas, Z. Phys. C **70** (1996) 435
21. A. Djouadi, W. Kilian, M. Muhlleitner, P.M. Zerwas, Higgs pair-production at high-energy colliders, XXIX Int. Conference on High Energy Physics, Vancouver 1998, Heidelberg Report HD-THEP 98-29; W. Kilian, P.M. Zerwas, Proceedings, XXIX Int. Conference on High Energy Physics, Vancouver 1998, [hep-ph/9809486]
22. M.N. Dubinin, A.V. Semenov, SNUTP-98-140 [hep-ph/9812246]
23. E. Accomando et al., Phys. Rep. **299** (1998) 1
24. K. Hübner, Proceedings, XXIX Int. Conference on High Energy Physics, Vancouver 1998; CERN Report CERN-SL-98-065 DI
25. R. Brinkmann, TESLA Collaboration, ECFA/DESY LC Workshop, Orsay 1998
26. S. Moretti, Rutherford Report, RAL-TR-98-035 [hep-ph/9808430]
27. See e.g. J. Kalinowski in: e^+e^-Collisions at 500 GeV: The Physics Potential, P.M. Zerwas ed., DESY 92-123A
28. D.J. Miller, S. Moretti, in preparation
29. K.J. Kallianpur, Phys. Lett. B **215** (1988) 392
30. G.L. Kane, W.W. Repko, W.B. Rolnick, Phys. Lett. B **148** (1984) 367; S. Dawson, Nucl. Phys. B **249** (1985) 42
31. E.E. Boos, M.N. Dubinin, V.A. Ilyin, A.E. Pukhov, V.I. Savrin, Report SNUTP-94-116 [hep-ph/9503280]; P.A. Baikov et al., *Proceedings of the Workshop QFTHEP-96*, eds. B. Levtchenko, V. Savrin, Moscow 1996, [hep-ph/9701412]
32. A. Djouadi, J. Kalinowski, P.M. Zerwas, Z. Phys. C **57** (1993) 569